SIAM Review
Vol. 56, No. 2, pp. 213–257

The Narrow Escape Problem*

D. Holcman†
Z. Schuss‡

Abstract. The narrow escape problem in diffusion theory is to calculate the mean first passage time of a diffusion process to a small target on the reflecting boundary of a bounded domain. The problem is equivalent to solving the mixed Dirichlet–Neumann boundary value problem for the Poisson equation with small Dirichlet and large Neumann parts. The mixed boundary value problem, which goes back to Lord Rayleigh, originates in the theory of sound and is closely connected to the eigenvalue problem for the mixed problem and for the Neumann problem in domains with bottlenecks. We review here recent developments in the nonstandard asymptotics of the problem, which are based on several ingredients: a better resolution of the singularity of Neumann's function, resolution of the boundary layer near the small target by conformal mappings of domains with bottlenecks, and the breakup of composite domains into simpler components. The new methodology applies to two- and higher-dimensional problems. Selected applications are reviewed.

Key words. diffusion processes, mean first passage time, narrow escape, Laplace equation, stochastic modeling, asymptotic expansions, Neumann's function, mixed Dirichlet–Neumann boundary value problem

AMS subject classifications. 15A15, 15A09, 15A23

DOI. 10.1137/120898395

1. Introduction.

The narrow escape problem in diffusion theory, which goes back to Helmholtz (Helmholtz (1860)) and Lord Rayleigh (Rayleigh (1945)) in the context of the theory of sound, is to calculate the mean first passage time (MFPT) of Brownian motion to a small absorbing window on the otherwise impermeable (reflecting) boundary of a bounded domain (see Figure 1.3). The renewed interest in the problem is due to the emergence of the narrow escape time (NET) as a key to the determination of biological cell function from its geometrical structure. The NET is ubiquitous in molecular and cellular biology and is manifested in stochastic models of chemical reactions (Holcman and Schuss (2005); Dao Duc and Holcman (2010)), in the computation of the synaptic current (Chen et al. (2000); Bredt and Nicoll (2003); Adesnik, Nicoll, and England (2005); Shi et al. (1999); Malinow and Malenka (2002); Malinow (2003); Earnshaw and Bressloff (2006); Holcman and Triller (2006); Ashby et al. (2006); Bressloff and Newby (2012)), in modeling the early steps of viral infection in cells, in the regulation of diffusion between the mother and daughter cells during division (Greber and Way (2006); Seisenberger et al. (2001); Gehlen et al. (2011)), and

*Received by the editors November 9, 2012; accepted for publication (in revised form) September 30, 2013; published electronically May 8, 2014.
http://www.siam.org/journals/sirev/56-2/89839.html

†Group of Applied Mathematics and Computational Biology, IBENS, Ecole Normale Supérieure, 75005 Paris, France (david.holcman@ens.fr). The research of this author was supported by an ERC Starting Grant.

‡Department of Applied Mathematics, Tel-Aviv University, Tel-Aviv 69978, Israel (schuss@post.tau.ac.il).

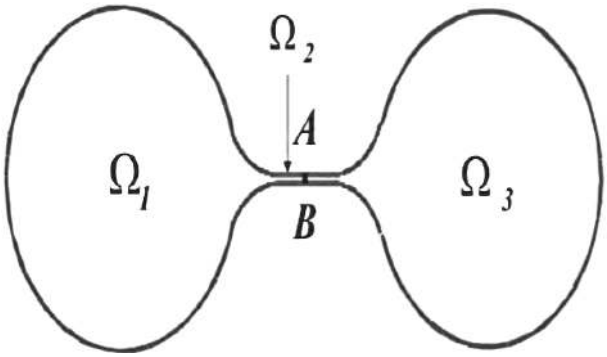

Fig. 1.1 *A dumbbell-shaped domain consists of two large compartments Ω_1 and Ω_3 connected by a narrow neck Ω_2. The bottleneck is the interval $\boldsymbol{AB}$.*

in many other models (see Holcman and Schuss (2013) and references therein). The NET coarse-grains diffusion from the molecular to the cellular scale: rare molecular events, such as ionic permeation through a protein channel of a biological membrane, give rise to channel current on the time scale of the NET.

The need to simulate several interacting species in a confined microdomain is manifested in the context of calcium dynamics in neuronal synapses. The number of molecules involved in the reaction is of the order of tens to hundreds. They are tracked with fluorescent dyes that drastically interfere with the reaction and diffusion processes. A similar situation arises in the simulation of synaptic transmission, starting with the arrival of neurotransmitter molecules at receptors on the postsynaptic membrane.

The microscopic model of reaction and diffusion, which is sensitive to geometrical features of the domain, can be coarse-grained into a Markovian jump process using the NET approximation. This approach takes advantage of the fact that the arrival process of Brownian particles from a practically infinite continuum to an absorbing target is Poissonian with rate that is the total flux on the absorbing boundary (Nadler, Naeh, and Schuss (2001); Schuss, Singer, and Holcman (2007); Schuss (2013)). The case of an absorbing sphere in an infinite domain with a fixed density of diffusers was worked out by Smoluchowski (Chandrasekhar (1943)). The rate constant, which is the reciprocal of the NET, coarse-grains the entire geometry to a single parameter. It is possible then to coarse-grain the binding and unbinding processes in microdomains into a Markov jump process, thus opening the way to full analysis of stochastic chemical reactions by providing closed-form formulas for the mean, variance, and any moments of interest of the process. This approach circumvents the complex reaction-diffusion partial differential equations that are much harder to solve.

Diffusion in structures interconnected by narrow passages, such as dumbbell-shaped domains (see Figure 1.1), is coarse-grained by the NET into a two-state Markovian jump process, whose transition rates are the reciprocals of the corresponding MFPTs. Specifically, in the symmetric case that $\Omega_1 = \Omega_3 = \Omega$ and the neck Ω_2 is of length L and radius a, the transition rate is given by

$$\frac{1}{\lambda_{\mathrm{I}\rightleftarrows\mathrm{II}}} = \sqrt{2}\left[\left(\frac{R_c}{a}\right)^{3/2}\frac{|\Omega|}{R_c D}\right][1+o(1)] + \frac{L^2}{4D} + \frac{|\Omega|L}{\pi a^2 D} \tag{1.1}$$

where D is the diffusion coefficient and R_c is the curvature of the boundary at the cusp. In this case the leading-order approximation to the principal eigenvalue of the Neumann problem for the Laplace equation in the dumbbell is $-(\lambda_{\mathrm{I}\to\mathrm{II}} + \lambda_{\mathrm{II}\to\mathrm{I}})$ (the general case is worked out in section 8.1.2).

The two-dimensional diffusion of receptors on a membrane crowded with obstacles can be modeled as diffusion outside a lattice of obstacles of radius a (see Figure 8.1). Figure 1.2(left) shows an elementary cell Ω. The NET from Ω, which is a domain with four cusp-like narrow passages of the type shown in Figure 4.1, is given in section 4.1 as

$$\bar{\tau} = \frac{\pi|\,\Omega|}{2D\sqrt{\varepsilon/a}}\,(1 + o(1)) \quad \text{for } \varepsilon \ll |\partial\Omega|, a, \tag{1.2}$$

where $\varepsilon = L - 2a$ is the gap between obstacles. The diffusion outside the lattice is coarse-grained by the NET into a Markovian jump process lattice of step L, whose rate is the reciprocal of the MFPT from one cell to another. The Markov process is coarse-grained, in turn, into a two-dimensional coarse diffusion process with an effective diffusion coefficient $D = 2L^2/\bar{\tau}$, where $\bar{\tau}$ is the MFPT to a single window $\partial\Omega_a$ when the others are closed (see Figure 1.2 and section 8.2).

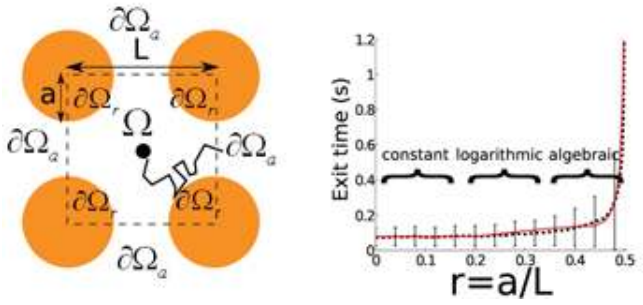

Fig. 1.2 *An elementary lattice cell Ω in a model of two-dimensional diffusion on a crowded membrane.* Left: *Brownian motion in Ω.* Right: NET *as a function of $r = a/L$ interpolated between three regions: constant, logarithmic, and* (1.2).

The main mathematical effort in the NET problem is to develop asymptotic methods for the approximate evaluation of the NET in the various geometries of cellular structures (see section 2). The problem is equivalent to the construction of an asymptotic solution to the homogeneous mixed Neumann–Dirichlet boundary value problem for the Poisson equation in a bounded domain.

The NET diverges as the Dirichlet part of the boundary shrinks, thus rendering the computation a singular perturbation problem. In two dimensions the problem is not the same as in higher dimensions, because the singularity of the Neumann function in two dimensions is logarithmic, while that in higher dimensions is algebraic. The computation is related to the calculation of the principal eigenvalue of the mixed Dirichlet–Neumann problem for the Laplace equation in the domain, when the Dirichlet boundary is only a small patch on the otherwise Neumann boundary. Specifically, the principal eigenvalue is asymptotically the reciprocal of the NET in the limit of shrinking patch. In this limit the escape of a Brownian trajectory becomes a rare event and is thus hard to track by Brownian dynamics simulations or other numerical methods due to the high dimension of the parameter space (see Figure 1.3). The purpose of this review is to present new singular perturbation methods that have been

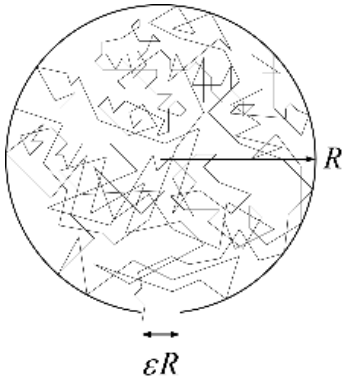

Fig. 1.3 *Brownian trajectory escaping through a small absorbing window in a domain with otherwise reflecting boundary.*

developed for the derivation of explicit analytical asymptotic approximations of the NET in this singular limit. Relevant references and history are reviewed at the end of each section.

1.1. References to Section 1. The narrow escape problem in diffusion theory was considered first by Lord Rayleigh in Rayleigh (1945) and elaborated upon in Fabrikant (1989, 1991); the terminology NET was introduced in Singer et al. (2006). A recent review of early results on the NET problem with many biological applications is given in Bressloff and Newby (2012) and in Holcman and Schuss (2013).

2. Formulation of the Narrow Escape Problem.

2.1. The Mixed Boundary Value Problem. Consider free Brownian motion in a bounded domain $D \subset \mathbb{R}^d$ ($d = 2, 3$), whose boundary $\partial\Omega$ is sufficiently smooth (the analysis in higher dimensions is similar to that for $d = 3$). The Brownian trajectory $\boldsymbol{x}(t)$ is reflected at the boundary, except for a small hole $\partial\Omega_a$, where it is absorbed, as shown in Figures 1.3 and 2.1(left). The reflecting part of the boundary is $\partial\Omega_r = \partial\Omega - \partial\Omega_a$. The lifetime in Ω of a Brownian trajectory that starts at a point $\boldsymbol{x} \in \Omega$ is the first passage time (FPT) τ of the trajectory to the absorbing boundary $\partial\Omega_a$. The NET

$$v(\boldsymbol{x}) = \mathbb{E}[\tau \,|\, \boldsymbol{x}(0) = \boldsymbol{x}] \tag{2.1}$$

is finite under quite general conditions (Schuss (2010b)). As the size (e.g., the diameter) of the absorbing hole decreases to zero, while that of the domain remains finite, the NET increases indefinitely. A measure of smallness can be chosen as the ratio between the surface area of the absorbing boundary and that of the entire boundary, for example,

$$\varepsilon = \left(\frac{|\partial\Omega_a|}{|\partial\Omega|}\right)^{1/(d-1)} \ll 1, \tag{2.2}$$

provided that the isoperimetric ratio remains bounded,

$$\frac{|\partial\Omega|^{1/(d-1)}}{|\Omega|^{1/d}} = O(1) \text{ for } \varepsilon \ll 1 \tag{2.3}$$

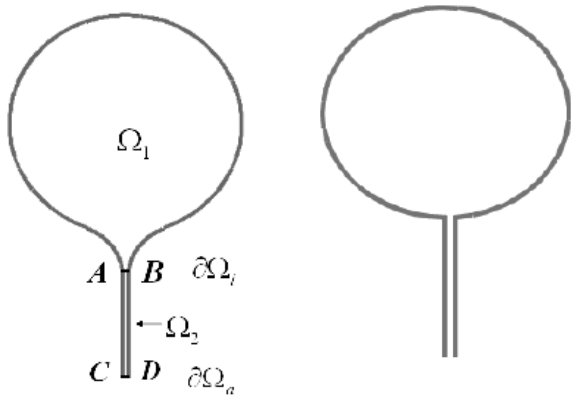

Fig. 2.1 *Mathematical idealizations of the cross-sections of neuronal spine morphologies as composite domains.* Left: *The bulky head Ω_1 is connected smoothly by an interface $\partial\Omega_i = AB$ to a narrow neck Ω_2. The entire boundary is $\partial\Omega_r$ (reflecting), except for a small absorbing part $\partial\Omega_a = CD$.* Right: *The head, shown separately in Figure* 1.3*, is connected to the neck without a funnel.*

(see the pathological example below when (2.3) is violated). The NET $v(\boldsymbol{x})$ satisfies the Pontryagin–Andronov–Vitt (PAV) mixed boundary value problem for the Poisson equation (Pontryagin, Andronov, and Vitt (1933, 1989); Schuss (2010b)),

$$\Delta v(\boldsymbol{x}) = -\frac{1}{D} \quad \text{for } \boldsymbol{x} \in \Omega, \tag{2.4}$$

$$v(\boldsymbol{x}) = 0 \quad \text{for } \boldsymbol{x} \in \partial\Omega_a, \tag{2.5}$$

$$\frac{\partial v(\boldsymbol{x})}{\partial n(\boldsymbol{x})} = 0 \quad \text{for } \boldsymbol{x} \in \partial\Omega_r, \tag{2.6}$$

where D is the diffusion coefficient and $\boldsymbol{n}(\boldsymbol{x})$ is the unit outer normal vector to the boundary at $\boldsymbol{x} \in \partial\Omega$. If Ω is a subset of a two-dimensional Riemannian manifold, as in Figure 2.2, the Laplace operator is replaced with the Laplace–Beltrami operator. The compatibility condition

$$\int_{\partial\Omega_a} \frac{\partial v(\boldsymbol{x})}{\partial n}\, dS_{\boldsymbol{x}} = -\frac{|\Omega|}{D} \tag{2.7}$$

is obtained by integrating (2.4) over Ω and using (2.5) and (2.6).

The solution $v(\boldsymbol{x})$ diverges to infinity as the hole shrinks to zero, e.g., as $\varepsilon \to 0$, except in a boundary layer near $\partial\Omega_a$, because the compatibility condition (2.7) fails in this limit. Our purpose here is to find an asymptotic approximation to $v(\boldsymbol{x})$ for small ε.

A Pathological Example. The following pathological example shows that when (2.3) is violated the NET does not necessarily increase to infinity as the relative area of the hole decreases to zero. This is illustrated by the following example. Consider a cylinder of length L and radius a. The boundary of the cylinder is reflecting, except for one of its bases (at $z = 0$, say), which is absorbing. The NET problem becomes

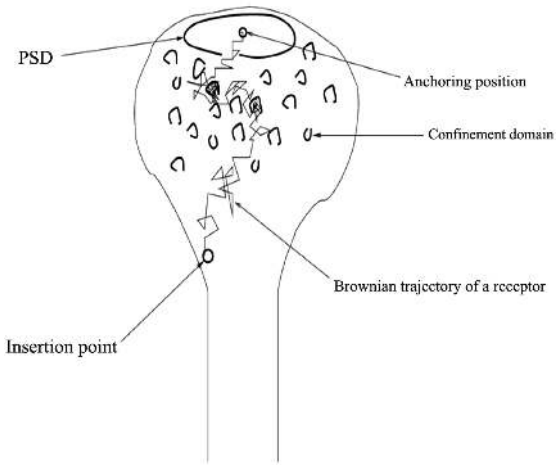

Fig. 2.2 *Receptor movement on the neuronal membrane.*

one-dimensional and its solution is

$$v(z) = Lz - \frac{z^2}{2}. \tag{2.8}$$

Here there is neither a boundary layer nor a constant outer solution; the NET grows gradually with z. The NET, averaged against a uniform initial distribution in the cylinder, is $\mathbb{E}\tau = L^2/3$ and is independent of a; that is, the assumption that the NET becomes infinite is violated. It holds, however, if the domain is sufficiently thick, e.g., when a ball of radius independent of ε can be rolled on the reflecting boundary inside the domain.

2.2. Neumann's Function and a Helmholtz Integral Equation. First, we prove the following theorem.

THEOREM 2.1 (the Helmholtz integral equation). *Under the assumption that the solution $v(\boldsymbol{x})$ of (2.4)–(2.6) diverges to infinity for all $\boldsymbol{x} \in \Omega$ as $\varepsilon \to 0$, the leading-order approximation to the boundary flux density*

$$g(\boldsymbol{x}) = \frac{\partial v(\boldsymbol{x})}{\partial n} \quad \textit{for } \boldsymbol{x} \in \partial\Omega_a \tag{2.9}$$

is the solution of the Helmholtz integral equation

$$\int_{\partial\Omega_a} N(\boldsymbol{x}, \boldsymbol{\xi}))g(\boldsymbol{x})\, dS_{\boldsymbol{x}} = -C_\varepsilon \quad \textit{for} \quad \boldsymbol{\xi} \in \partial\Omega_a \tag{2.10}$$

for some constant C_ε.

Proof. To calculate the NET $v(\boldsymbol{x})$, we use the Neumann function $N(\boldsymbol{x}, \boldsymbol{\xi})$, which is a solution of the boundary value problem

$$\begin{aligned} \Delta_{\boldsymbol{x}} N(\boldsymbol{x}, \boldsymbol{\xi}) &= -\,\delta(\boldsymbol{x} - \boldsymbol{\xi}) \quad \text{for } \boldsymbol{x}, \boldsymbol{\xi} \in \Omega, \\ \frac{\partial N(\boldsymbol{x}, \boldsymbol{\xi})}{\partial n(\boldsymbol{x})} &= -\,\frac{1}{|\partial\Omega|} \quad \text{for } \boldsymbol{x} \in \partial\Omega, \boldsymbol{\xi} \in \Omega, \end{aligned} \tag{2.11}$$

and is defined up to an additive constant. Green's identity gives

$$\int_\Omega [N(\boldsymbol{x},\boldsymbol{\xi})\Delta v(\boldsymbol{x}) - v(\boldsymbol{x})\Delta N(\boldsymbol{x},\boldsymbol{\xi})]\, d\boldsymbol{x} = \int_{\partial\Omega} \left[N(\boldsymbol{x},\boldsymbol{\xi})\frac{\partial v(\boldsymbol{x})}{\partial n} - v(\boldsymbol{x})\frac{\partial N(\boldsymbol{x},\boldsymbol{\xi})}{\partial n}\right] dS_{\boldsymbol{x}}$$
$$= \int_{\partial\Omega} N(\boldsymbol{x},\boldsymbol{\xi})\frac{\partial v(\boldsymbol{x})}{\partial n}\, dS_{\boldsymbol{x}} + \frac{1}{|\partial\Omega|}\int_{\partial\Omega} v(\boldsymbol{x})\, dS_{\boldsymbol{x}}.$$

On the other hand, (2.4) and (2.11) imply that

$$\int_\Omega [N(\boldsymbol{x},\boldsymbol{\xi})\Delta v(\boldsymbol{x}) - v(\boldsymbol{x})\Delta N(\boldsymbol{x},\boldsymbol{\xi})]\, d\boldsymbol{x} = v(\boldsymbol{\xi}) - \frac{1}{D}\int_\Omega N(\boldsymbol{x},\boldsymbol{\xi})\, d\boldsymbol{x},$$

hence

$$v(\boldsymbol{\xi}) - \frac{1}{D}\int_\Omega N(\boldsymbol{x},\boldsymbol{\xi})\, d\boldsymbol{x} = \int_{\partial\Omega} N(\boldsymbol{x},\boldsymbol{\xi})\frac{\partial v(\boldsymbol{x})}{\partial n}\, dS_{\boldsymbol{x}} + \frac{1}{|\partial\Omega|}\int_{\partial\Omega} v(\boldsymbol{x})\, dS_{\boldsymbol{x}}. \tag{2.12}$$

Note that the second integral on the right-hand side of (2.12) is an additive constant. The integral

$$C_\varepsilon = \frac{1}{|\partial\Omega|}\int_{\partial\Omega} v(\boldsymbol{x})\, dS_{\boldsymbol{x}} \tag{2.13}$$

is the average of the NET on the boundary. Now (2.12) takes the form

$$v(\boldsymbol{\xi}) = \frac{1}{D}\int_\Omega N(\boldsymbol{x},\boldsymbol{\xi})\, d\boldsymbol{x} + \int_{\partial\Omega_a} N(\boldsymbol{x},\boldsymbol{\xi})\frac{\partial v(\boldsymbol{x})}{\partial n}\, dS_{\boldsymbol{x}} + C_\varepsilon, \tag{2.14}$$

which is an integral representation of $v(\boldsymbol{\xi})$. We use the boundary condition (2.5) and (2.9) to write (2.14) as

$$0 = \frac{1}{D}\int_\Omega N(\boldsymbol{x},\boldsymbol{\xi})\, d\boldsymbol{x} + \int_{\partial\Omega_a} N(\boldsymbol{x},\boldsymbol{\xi})g(\boldsymbol{x})\, dS_{\boldsymbol{x}} + C_\varepsilon \tag{2.15}$$

for all $\boldsymbol{\xi} \in \partial\Omega_a$. Equation (2.15) is an integral equation for $g(\boldsymbol{x})$ and C_ε. To construct an asymptotic approximation to the solution, we note that the first integral in (2.15) is a regular function of $\boldsymbol{\xi}$ on the boundary. Indeed, due to the symmetry of the Neumann function, we have from (2.11)

$$\Delta_{\boldsymbol{\xi}}\int_\Omega N(\boldsymbol{x},\boldsymbol{\xi})\, d\boldsymbol{x} = -1 \ \text{ for } \ \boldsymbol{\xi} \in \Omega \tag{2.16}$$

and

$$\frac{\partial}{\partial n(\boldsymbol{\xi})}\int_\Omega N(\boldsymbol{x},\boldsymbol{\xi})\, d\boldsymbol{x} = -\frac{|\Omega|}{|\partial\Omega|} \ \text{ for } \ \boldsymbol{\xi} \in \partial\Omega. \tag{2.17}$$

Equation (2.16) and the boundary condition (2.17) are independent of the hole $\partial\Omega_a$, so they define the first integral on the right-hand side of (2.15) as a regular function of $\boldsymbol{\xi}$, up to an additive constant, also independent of $\partial\Omega_a$.

The assumption that for all $\boldsymbol{x} \in \Omega$ the NET $v(\boldsymbol{x})$ diverges to infinity as $\varepsilon \to 0$ in (2.13) implies that $C_\varepsilon \to \infty$ in this limit. This means that for $\boldsymbol{\xi} \in \partial\Omega_a$ the second integral in (2.15) must also become infinite in this limit, because the first integral is independent of $\partial\Omega_a$. Therefore, the leading-order approximation to the solution $g(\boldsymbol{x})$ of the integral equation (2.15) is the solution of (2.10). ∎

3. NET on a Two-Dimensional Riemannian Manifold. We consider a Brownian trajectory $\boldsymbol{x}(t)$ in a bounded domain Ω on a two-dimensional Riemannian manifold (Σ, g) (see relevant references in section 1.1). For a domain $\Omega \subset \Sigma$ with a smooth boundary $\partial\Omega$ (at least C^1), we denote by $|\Omega|_g$ the Riemannian surface area of Ω and by $|\partial\Omega|_g$ the arclength of its boundary, computed with respect to the metric g. As in the previous section, the boundary $\partial\Omega$ is partitioned into an absorbing arc $\partial\Omega_a$ and the remaining part $\partial\Omega_r = \partial\Omega - \partial\Omega_a$ is reflecting for the Brownian trajectories. We assume that the absorbing part is small, that is, (2.2) holds in the form

$$\varepsilon = \frac{|\partial\Omega_a|_g}{|\partial\Omega|_g} \ll 1;$$

however, Σ and Ω are independent of ε, and only the partition of the boundary $\partial\Omega$ into absorbing and reflecting parts varies with ε. The FPT τ of the Brownian motion from Ω to $\partial\Omega_a$ has a finite mean $u(\boldsymbol{x}) = \mathbb{E}[\tau \,|\, \boldsymbol{x}(0) = \boldsymbol{x}]$ and the function $u(\boldsymbol{x})$ satisfies the mixed Neumann–Dirichlet boundary value problem (2.4)–(2.6), which is now written as

$$D\Delta_g u(\boldsymbol{x}) = -1 \ \text{ for } \boldsymbol{x} \in \Omega, \tag{3.1}$$

$$\frac{\partial u(\boldsymbol{x})}{\partial n} = 0, \ \text{ for } \boldsymbol{x} \in \partial\Omega - \partial\Omega_a, \tag{3.2}$$

$$u(\boldsymbol{x}) = 0 \quad \text{for for } \boldsymbol{x} \in \partial\Omega_a, \tag{3.3}$$

where D is the diffusion coefficient and Δ_g is the Laplace–Beltrami operator on Σ

$$\Delta_g f = \frac{1}{\sqrt{\det G}} \sum_{i,j} \frac{\partial}{\partial \xi_i} \left(g^{ij} \sqrt{\det G} \frac{\partial f}{\partial \xi_j} \right), \tag{3.4}$$

with

$$\boldsymbol{t}_i = \frac{\partial |\boldsymbol{x}|}{\partial \xi_i}, \quad g_{ij} = \langle \boldsymbol{t}_i, \boldsymbol{t}_j \rangle, \quad G = (g_{ij}), \quad g^{ij} = g_{ij}^{-1}. \tag{3.5}$$

Obviously, $u(\boldsymbol{x}) \to \infty$ as $\varepsilon \to 0$, except for $\boldsymbol{x}$ in a boundary layer near $\partial\Omega_a$.

THEOREM 3.1. *Under the assumptions spelled out at the beginning of this section, the* NET *is given by*

$$\mathbb{E}[\tau \,|\, \boldsymbol{x}] = u(\boldsymbol{x}) = \frac{|\Omega|_g}{\pi D} \left[\log \frac{1}{\varepsilon} + O(1) \right] \quad \textit{for } \varepsilon \ll 1. \tag{3.6}$$

Proof. We fix the origin $\mathbf{0} \in \partial\Omega_a$ and represent the boundary curve $\partial\Omega$ in terms of arclength s as $(x(s), y(s))$ and rescale s so that

$$\partial\Omega = \left\{ (x(s), y(s)) \,:\, -\frac{1}{2} < s \le \frac{1}{2} \right\}, \ \left(x\left(-\frac{1}{2}\right), y\left(-\frac{1}{2}\right) \right) = \left(x\left(\frac{1}{2}\right), y\left(\frac{1}{2}\right) \right).$$

We assume that the functions $x(s)$ and $y(s)$ are real analytic in the interval $2|s| < 1$ and that the absorbing part of the boundary $\partial\Omega_a$ is the arc

$$\partial\Omega_a = \{ (x(s), y(s)) \,:\, |s| < \varepsilon \}.$$

The Neumann function can be written as

$$N(\boldsymbol{x},\boldsymbol{\xi}) = -\frac{1}{2\pi}\log d(\boldsymbol{x},\boldsymbol{\xi}) + v_N(\boldsymbol{x},\boldsymbol{\xi}) \text{ for } \boldsymbol{x}\in B_\delta(\boldsymbol{\xi}), \tag{3.7}$$

where $B_\delta(\boldsymbol{\xi})$ is a geodesic ball of radius δ centered at $\boldsymbol{\xi}$ and $v_N(\boldsymbol{x};\boldsymbol{\xi})$ is a regular function (Garabedian (1964); Aubin (1998); Gilbarg and Trudinger (2001)). We consider a normal geodesic coordinate system (x, y) at the origin, such that one of the coordinates coincides with the tangent coordinate to $\partial\Omega_a$. We choose unit vectors $\boldsymbol{e}_1, \boldsymbol{e}_2$ as an orthogonal basis in the tangent plane at 0 so that for any vector field $\boldsymbol{X} = x_1\boldsymbol{e}_1 + x_2\boldsymbol{e}_2$, the metric tensor g can be written as

$$g_{ij} = \delta_{ij} + \varepsilon^2 \sum_{kl} a_{ij}^{kl} x_k x_l + o(\varepsilon^2), \tag{3.8}$$

where $|x_k| \le 1$, because ε is small. It follows that for $\boldsymbol{x}, \boldsymbol{y}$ inside the geodesic ball of radius ε, centered at the origin, $d(\boldsymbol{x},\boldsymbol{y}) = d_E(\boldsymbol{x},\boldsymbol{y}) + O(\varepsilon^2)$, where d_E is the Euclidean metric.

To construct an asymptotic expansion of the solution of (2.10) for small ε, we recall that when both $\boldsymbol{x}$ and $\boldsymbol{\xi}$ are on the boundary, $v_N(\boldsymbol{x},\boldsymbol{\xi})$ becomes singular (see Garabedian (1964, p. 247, equation (7.46))) and the singular part gains a factor of 2, due to the singularity of the "image charge." Denoting by $\tilde{v}_N$ the new regular part, (2.10) becomes

$$\int_{|s'|<\varepsilon} \left[\tilde{v}_N(\boldsymbol{x}(s');\boldsymbol{\xi}(s)) - \frac{\log d(\boldsymbol{x}(s),\boldsymbol{\xi}(s'))}{\pi}\right] f(s')\, S(ds') = C_\varepsilon, \tag{3.9}$$

where $S(ds')$ is the induced measure element on the boundary, $\boldsymbol{x} = (x(s), y(s))$, $\boldsymbol{\xi} = (\xi(s), \eta(s))$, and $f(s') = g_0(\boldsymbol{x}(s'))$. Expanding all functions in powers of ε and then in powers of s and s' for $|s|, |s'| < \varepsilon$, the integrals give at the leading order (see Holcman and Schuss (2004); Singer, Schuss, and Holcman (2006b); Schuss (2013) for details of the computation)

$$\varepsilon\,(\log\varepsilon - 1)\, f_0 + \sum_p \left(\frac{\varepsilon^{2p+1}}{2p+1}\log\varepsilon - \frac{\varepsilon^{2p+1}}{(2p+1)^2}\right) f_{2p} = \frac{\pi}{2}\int_{-\varepsilon}^{\varepsilon} v_0(s')\, ds' + C_\varepsilon, \tag{3.10}$$

where f_n are the Taylor coefficients of $f(s)$ and $v_n(s)$ are the coefficients in the expansion of $v(s)$ in powers of ε. Equation (3.10) and

$$\frac{1}{2}\int_{-\varepsilon}^{\varepsilon} f(s)\, S(ds) = \sum_p \frac{\varepsilon^{2p+1}}{(2p+1)} f_{2p}$$

determine the leading-order term in the expansion of C_ε. Indeed, the compatibility condition (2.7) gives

$$\int_{-\varepsilon}^{\varepsilon} f(s)\, S(ds) = -|\Omega|_g, \tag{3.11}$$

so using the fact that $\int_{-\varepsilon}^{\varepsilon} v_0(s')S(ds') = O(\varepsilon)$, we find that the leading-order expansion of C_ε in (3.10) is

$$C_\varepsilon = \frac{|\Omega|_g}{\pi}\left[\log\frac{1}{\varepsilon} + O(1)\right] \quad \text{for } \varepsilon \ll 1. \tag{3.12}$$

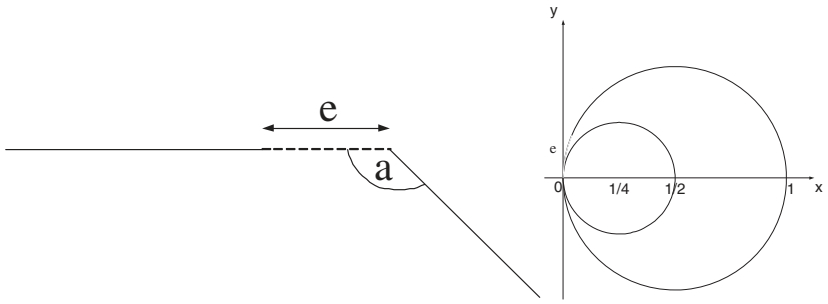

Fig. 3.1 Left: *A small opening near a corner of angle* α. Right: *The point* $(0,0)$ *is a cusp point of the dotted domain bounded between the two circles. The small absorbing arc of length* ε *is located at the cusp point.*

If the diffusion coefficient is D, (2.10) gives the NET from a point $\boldsymbol{x} \in \Omega$, outside the boundary layer, as

$$\mathbb{E}[\tau \,|\, \boldsymbol{x}] = u(\boldsymbol{x}) = \frac{|\Omega|_g}{\pi D}\left[\log\frac{1}{\varepsilon} + O(1)\right] \quad \text{for } \varepsilon \ll 1. \tag{3.13}$$

Note that it is enough to assume that the boundary is of class C^1 and the metric is of class C^2 to obtain a leading-order expansion. □

3.1. Exit near Singularities of the Boundary. If the window is at a corner of an opening angle α in the boundary (see Figure 3.1(left)), the NET is to leading order

$$\mathbb{E}\tau = \frac{|\Omega|}{D\alpha}\left[\log\frac{1}{\varepsilon} + O(1)\right]. \tag{3.14}$$

Indeed, putting the origin at the apex of the angle and the real axis on one of the rays of the angle, the conformal mapping $z \mapsto z^{\pi/\alpha}$ of Ω flattens the corner and leaves $\partial\Omega_a$ small. The Neumann function for the upper half plane, $\pi^{-1}\log z$, is transformed into $\alpha^{-1}\log z$, so (3.13) gives (3.14).

To see that the area factor $|\Omega|$ remains unchanged under any conformal mapping $f : (x,y) \mapsto (u(x,y), v(x,y))$, we note that this factor is a consequence of the compatibility condition (2.7), which relates the area to the integral

$$\int_\Omega \Delta_{(x,y)} w \, dx\, dy = -\frac{|\Omega|}{D},$$

where $w(x,y) = \mathbb{E}[\tau |\, x(0) = x, y(0) = y]$ satisfies $\Delta_{(x,y)} w = -1/D$. According to the Cauchy–Riemann equation the Laplacian transforms as

$$\Delta_{(x,y)} w = (u_x^2 + u_y^2)\Delta_{(u,v)} w$$

and the Jacobian of the transformation is $J = u_x^2 + u_y^2$. Therefore,

$$\int_\Omega \Delta_{(x,y)} w \, dx\, dy = \int_{f(\Omega)} \Delta_{(u,v)} w \, du\, dv.$$

This means that the compatibility condition remains unchanged and gives the area of the original domain. Higher-order asymptotics are given in Singer, Schuss, and Holcman (2006b).

If the absorbing arc is at a cusp of the boundary, the leading-order term of the asymptotic expansion of the NET can be found by mapping the domain conformally onto the upper half plane. A cusp can be viewed as a corner with opening angle $\alpha = 0$, so a different asymptotic expansion than (3.14) should be expected. Consider, for example, Brownian motion in a domain enclosed between the circles $(x-1/2)^2+y^2 = 1/4$ and $(x-1/4)^2+y^2 = 1/16$ (see Figure 3.1(right)).

The conformal mapping $z \mapsto \exp\{\pi i(1/z-1)\}$ maps this domain onto the upper half plane. Therefore, the NET is to leading order

$$\mathbb{E}\tau = \frac{|\Omega|}{D}\left[\frac{1}{\varepsilon} + O(1)\right]. \tag{3.15}$$

3.2. NET on a Two-Dimensional Sphere. Another example is that of Brownian motion on the surface of a 3-sphere of radius R, described by the spherical coordinates (θ, ϕ),

$$x = R\sin\theta\cos\phi, \quad y = R\sin\theta\sin\phi, \quad z = R\cos\theta.$$

In spherical coordinates (3.4) and (3.5) give (John (1982))

$$g_{\theta\theta} = R^2, \quad g_{\phi\phi} = R^2\sin^2\theta, \quad g_{\theta\phi} = g_{\phi\theta} = 0. \tag{3.16}$$

Therefore, for a function on the 3-sphere $w = w(\theta, \phi)$ the Laplace–Beltrami operator Δ_M is given by

$$\Delta_M f = R^{-2}\left(\frac{\partial^2 f}{\partial\theta^2} + \cot\theta\,\frac{\partial f}{\partial\theta} + \frac{1}{\sin^2\theta}\frac{\partial^2 f}{\partial\phi^2}\right).$$

If the Brownian motion is absorbed when it reaches a small spherical cap centered at the north pole $\theta = 0$ with a small opening angle δ (see Figure 3.2), the MFPT to the cap, $v(\theta)$, satisfies the PAV boundary value problem

$$\Delta_M v = R^{-2}\left(v'' + \cot\theta\, v'\right) = -1, \tag{3.17}$$

$$v'(\pi) = 0, \quad v(\delta) = 0, \tag{3.18}$$

because, due to rotational symmetry, the FPT to the spherical cap is independent of the initial angle ϕ. The solution of the boundary value problem (3.17)–(3.18) is given by

$$v(\theta) = 2R^2\log\frac{\sin\frac{\theta}{2}}{\sin\frac{\delta}{2}}. \tag{3.19}$$

A different approach to the calculation of the MFPT of Brownian motion on the 3-sphere is based the stereographic projection of the sphere onto the plane (Hille (1976)). A related problem is that of entering a circular corral on the 3-sphere through a small arc. These cases are discussed in Singer, Schuss, and Holcman (2006a) and Schuss (2013). A general approach leading to explicit asymptotic computations and valid for several holes uses matched asymptotics (see Cheviakov, Ward, and Straube (2010) and the next section).

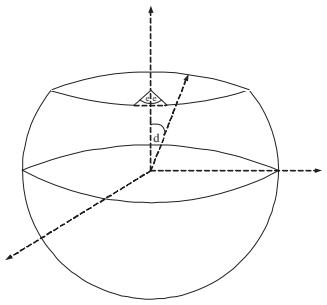

Fig. 3.2 *A sphere of radius R without a spherical cap at the north pole with central angle δ. The Brownian motion is absorbed at the boundary of the cap or only at an arc of length 2ε on the boundary of the cap.*

3.3. The Matched Asymptotics Approach. In the matched asymptotics approach to the NET problem from a domain Ω in $\mathbb{R}^2$, a boundary layer solution is constructed near an absorbing window $\partial\Omega_a$ of size 2ε (Ward, Henshaw, and Keller (1993); Pillay et al. (2010)). First, the mixed boundary value problem (2.4)–(2.6) is converted to local coordinates (η, s), where η is the distance of a point $\boldsymbol{x} \in \Omega$ from the boundary $\partial\Omega$ and s is arclength from the center of the window to the orthogonal projection of $\boldsymbol{x}$ on $\partial\Omega$. If $\partial\Omega$ is sufficiently smooth in a neighborhood of the window $\partial\Omega_a$, (2.4) for the MFPT $v(\boldsymbol{x})$ is converted locally to

$$w_{\eta\eta} - \frac{\kappa}{1-\kappa\eta} w_\eta + \frac{1}{1-\kappa\eta}\left(\frac{1}{1-\kappa\eta} w_s\right)_s = -\frac{1}{D}, \tag{3.20}$$

where $w(\eta, s) = v(\boldsymbol{x})$ and κ is the boundary curvature at the projection of $\boldsymbol{x}$ on $\partial\Omega$. If s is measured from the center of the arc $\partial\Omega_a$, the stretching $\eta = \varepsilon\hat{\eta},\ s = \varepsilon\hat{s}$, $\hat{w}(\hat{\eta}, \hat{s}) = w(\eta, s)$ maps a boundary strip near $\partial\Omega_a$ into the upper half plane. Assuming, as we may, that the origin $\boldsymbol{x} = \boldsymbol{0}$ is at the center of $\partial\Omega_a$, we set $\boldsymbol{y} = \boldsymbol{x}/\varepsilon = (\hat{\eta}, \hat{s})$. An expansion in powers of ε gives the leading-order boundary layer problem for (2.4)–(2.6) as

$$\hat{w}_{\mathrm{BL},\hat{\eta}\hat{\eta}} + \hat{w}_{\mathrm{BL},\hat{s}\hat{s}} = 0 \ \text{ for } 0 < \hat{\eta} < \infty,\ -\infty < \hat{s} < \infty, \tag{3.21}$$

$$\hat{w}_{\mathrm{BL},\hat{\eta}}(0, \hat{s}) = 0 \ \text{ for } |\hat{s}| > 1, \quad \hat{w}_{\mathrm{BL}}(0, \hat{s}) = 0 \ \text{ for } |\hat{s}| < 1. \tag{3.22}$$

We specify the growth condition $\hat{w}_{\mathrm{BL}} \sim A \log|\boldsymbol{y}|$ as $|\boldsymbol{y}| \to \infty$, where A is an as yet undetermined constant. Setting $z = \hat{s} + i\hat{\eta}$, the transformation $\zeta = u + iv = \mathrm{Arcsin}\, z = -i\mathrm{Log}\,[iz + \sqrt{1-z^2}]$ maps the upper half plane $\hat{\eta} > 0$ onto the semi-infinite strip $\hat{\Omega} = \{-\pi/2 < u < \pi/2,\ 0 < v < \infty\}$. The mixed boundary value problem (3.21)–(3.22) is transformed into

$$\hat{W}_{uu}(u, v) + \hat{W}_{vv}(u, v) = 0 \ \text{ for } (u, v) \in \hat{\Omega},$$

$$\hat{W}_u\left(\pm\frac{\pi}{2}, v\right) = 0 \ \text{ for } 0 < v < \infty,$$

$$\hat{W}(u, 0) = 0 \ \text{ for } -\frac{\pi}{2} < u < \frac{\pi}{2},$$

where $\hat{W}(u, v) = \hat{w}_{\mathrm{BL}}(\hat{\eta}, \hat{s})$. The solutions $\hat{W}(u, v) = Av$ have the required logarithmic behavior for $|\boldsymbol{y}| \to \infty$, specifically,

$$\hat{w}_{\mathrm{BL}} \sim A \log|\boldsymbol{y}| + \log 2 + o(1) \ \text{ as } |\boldsymbol{y}| \to \infty. \tag{3.23}$$

The constant A is related to the boundary flux by $A = 2\pi^{-1} \int_0^1 \hat{w}_{\mathrm{BL},\hat{\eta}}(0, \hat{s})\, d\hat{s}$.

The leading term $w_{\text{OUT}}(\boldsymbol{x})$ in the outer expansion satisfies the original equation with the reduced boundary condition and the matching condition

$$\begin{aligned}
\Delta_{\boldsymbol{x}} w_{\text{OUT}}(\boldsymbol{x}) &= -\frac{1}{D} \text{ for } \boldsymbol{x} \in \Omega, \\
\frac{\partial w_{\text{OUT}}(\boldsymbol{x})}{\partial n} &= 0 \text{ for } \boldsymbol{x} \in \partial\Omega - \{\mathbf{0}\}, \\
w_{\text{OUT}}(\boldsymbol{x}) &\sim A\left[\log\left(\frac{1}{\varepsilon}\right) + \log 2 + \log|\boldsymbol{x}|\right] \text{ for } \boldsymbol{x} \to \mathbf{0}.
\end{aligned}$$

Then the compatibility condition (2.7) gives (3.13).

3.4. References to Sections 2 and 3. In the matched asymptotics approach to the NET problem from a domain Ω in $\mathbb{R}^2$, a boundary layer solution is constructed near an absorbing window $\partial\Omega_a$ of size 2ε (Ward, Henshaw, and Keller (1993); Pillay et al. (2010)). The method was developed in Ward and Keller (1993); Ward, Henshaw, and Keller (1993); Ward and Van De Velde (1992); Kolokolnikov, Titcombe, and Ward (2005); and Cheviakov, Ward, and Straube (2010). In three dimensions the method was used in Ward and Keller (1993), where the boundary layer problem is the classical electrified disk problem (Jackson (1975)). Further refinements of (3.13) are given in Ward and Keller (1993); Ward, Henshaw, and Keller (1993); Ward and Van De Velde (1992); Kolokolnikov, Titcombe, and Ward (2005); Cheviakov, Ward, and Straube (2010); Singer, Schuss, and Holcman (2006a); and Schuss, Singer, and Holcman (2007).

The NET calculated in section 2 was calculated for small absorbing windows in a smooth reflecting boundary in Ward and Keller (1993); Ward, Henshaw, and Keller (1993); Ward and Van De Velde (1992); Kolokolnikov, Titcombe, and Ward (2005); Cheviakov, Ward, and Straube (2010); Coombs, Straube, and Ward (2009); Grigoriev et al. (2002); Holcman and Schuss (2004); Singer et al. (2006); Singer, Schuss, and Holcman (2006a,b); Singer and Schuss (2006); Bénichou and Voituriez (2008); Schuss, Singer, and Holcman (2007); Gandolfi, Gerardi, and Marchetti (1985); and others. Several more complex cases, such as the NET through a window at a corner or at a cusp in the boundary and the NET on Riemannian manifolds, were considered in Singer et al. (2006) and Singer, Schuss, and Holcman (2006a,b). Exit through many holes is discussed in Holcman and Schuss (2008b,a); Holcman and Schuss (2012); Cheviakov, Ward, and Straube (2010); and references therein.

4. Brownian Motion in Dire Straits. In this section we consider Brownian motion in two-dimensional domains whose boundaries are smooth and reflecting, except for a small absorbing window at the end of a cusp-shaped funnel, as shown in Figures 2.1(left) and 4.1 (see references in section 4.5). The cusp can be formed by a partial block of a planar domain, as shown in Figure 4.2(left). The MFPT from $\boldsymbol{x} \in \Omega$ to the absorbing boundary $\partial\Omega_a$, denoted $\bar{\tau}_{\boldsymbol{x}\to\partial\Omega_a}$, is the NET from the domain Ω to the small window $\partial\Omega_a$ (of length a), such that

$$\varepsilon = \frac{\pi|\partial\Omega_a|}{|\partial\Omega|} = \frac{\pi a}{|\partial\Omega|} \ll 1. \tag{4.1}$$

4.1. The MFPT to a Bottleneck. We consider the NET problem in an asymmetric planar domain, as in Figure 4.2(left) or in an asymmetric version of the (dimensional) domain Ω' in Figure 4.1(left). We use the (dimensional) representation of

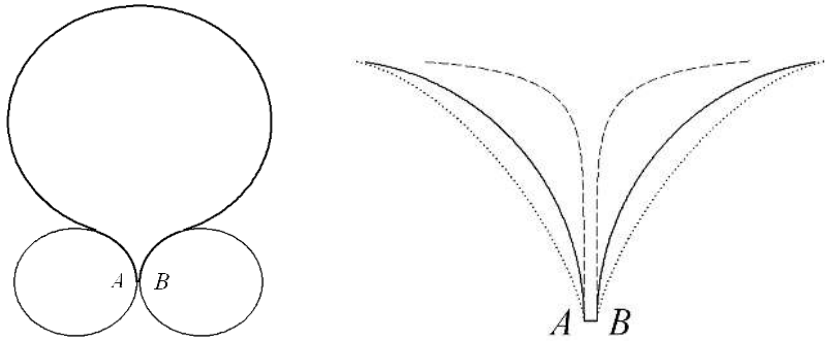

Fig. 4.1 Left: *The planar (dimensional) domain Ω' is bounded by a large circular arc connected smoothly to a funnel formed by moving two tangent circular arcs of radius R_c ε apart (i.e., $\overline{AB} = \varepsilon$).* Right: *Blowup of the cusp region. The solid, dashed, and dotted necks correspond to $\nu_\pm = 1$, 0.4, and 5 in* (4.3)*, respectively.*

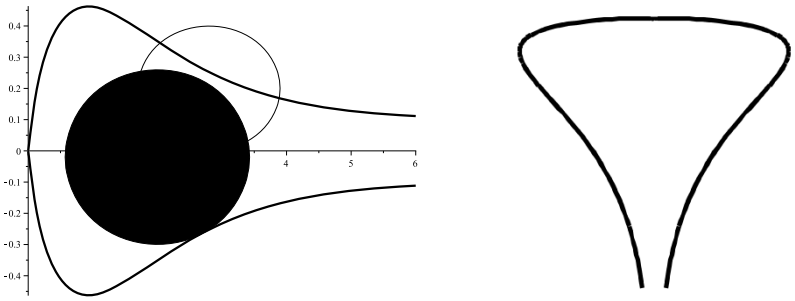

Fig. 4.2 Left: *Narrow straits formed by a partial block (solid disk) of the passage from the head to the neck of the domain enclosed by the black line. Inside the circle the narrow straits can be approximated by the gap between adjacent circles.* Right: *A surface of revolution with a funnel. The z-axis points down.*

the boundary curves for the upper and lower parts, respectively,

$$y' = r_\pm(x'),\ \Lambda' < x' < 0, \tag{4.2}$$

where the x'-axis is horizontal with $x' = \Lambda'$ at AB. We assume that the parts of the curve that generate the funnel have the form

$$\begin{aligned} r_\pm(x') &= O(\sqrt{|x'|}) \ \text{ near } x' = 0, \\ r_\pm(x') &= \pm a' \pm \frac{(x' - \Lambda')^{1+\nu_\pm}}{\nu_\pm(1+\nu_\pm)\ell_\pm^{\nu_\pm}}(1 + o(1)) \ \text{ for } \nu_\pm > 0 \text{ near } x' = \Lambda', \end{aligned} \tag{4.3}$$

where $a' = \frac{1}{2}\overline{AB} = \varepsilon'/2$ is the radius of the gap, and the constants $\ell_\pm$ have dimension of length. For $\nu_\pm = 1$ the parameters $\ell_\pm$ are the radii of curvature $R_c^\pm$ at $x' = \Lambda'$. To simplify the conformal mapping, we first rotate the domain by $\pi/2$ clockwise to assume the shape in Figure 4.2(right). The rotated axes are renamed (x', y') as well.

THEOREM 4.1 (the MFPT to a bottleneck). *The* NET *of Brownian motion to the end of the bottleneck at $x' = \Lambda'$ in the domain Ω' bounded by the curves* (4.2) and

(4.3) *is given by*

$$\bar{\tau} \sim \frac{\pi|\Omega'|}{2D\sqrt{\tilde{\varepsilon}}}, \tag{4.4}$$

where $\tilde{\varepsilon} = 2r_c\varepsilon/(R_c + r_c)$. *In dimensional units* (4.4) *is*

$$\bar{\tau} = \sqrt{\frac{R_c(R_c + r_c)}{2r_c\varepsilon'}}\frac{\pi|\,\Omega'|}{2D}\,(1 + o(1)) \quad \textit{for } \varepsilon' \ll |\partial\Omega'|, R_c, r_c. \tag{4.5}$$

In the symmetric case $R_c = r_c$ (4.5) *reduces to*

$$\bar{\tau} = \frac{\pi|\,\Omega'|}{2D\sqrt{\varepsilon'/R_c}}\,(1 + o(1)) \quad \textit{for } \varepsilon' \ll |\partial\Omega'|, R_c. \tag{4.6}$$

Proof. We consider Brownian motion in a domain Ω' with diffusion coefficient D and with reflection at the boundary $\partial\Omega'$, except for an absorbing boundary $\partial\Omega'_a$ at the bottom of the neck. The MFPT from a point $\boldsymbol{x}' = (x', y')$ inside the domain Ω' to $\partial\Omega'_a$ is the solution of the PAV boundary value problem (2.4)–(2.6), which we rewrite in dimensional variables as

$$\begin{aligned} &D\Delta\bar{u}(\boldsymbol{x}') = -1 \text{ for } \boldsymbol{x}' \in \Omega', \\ &\frac{\partial\bar{u}(\boldsymbol{x}')}{\partial n} = 0 \text{ for } \boldsymbol{x}' \in \partial\Omega' - \partial\Omega'_a, \quad \bar{u}(\boldsymbol{x}') = 0 \text{ for } \boldsymbol{x}' \in \partial\Omega'_a. \end{aligned} \tag{4.7}$$

Converting to dimensionless variables by setting $\boldsymbol{x}' = \ell_+\boldsymbol{x}$, $\Lambda' = \ell_+\Lambda$, the domain Ω' is mapped into Ω and we have (see (4.8) below)

$$|\Omega'| = \ell_+^2|\Omega|, \ |\partial\Omega'| = \ell_+|\partial\Omega|, \ |\partial\Omega'_a| = \varepsilon' = \ell_+|\partial\Omega_a| = \ell_+\varepsilon. \tag{4.8}$$

Setting $\bar{u}(\boldsymbol{x}') = u(\boldsymbol{x})$, we write (4.7) as

$$\begin{aligned} &\frac{D}{\ell_+^2}\Delta u(\boldsymbol{x}) = -1 \text{ for } \boldsymbol{x} \in \Omega, \\ &\frac{\partial u(\boldsymbol{x})}{\partial n} = 0 \text{ for } \boldsymbol{x} \in \partial\Omega - \partial\Omega_a, \quad u(\boldsymbol{x}) = 0 \text{ for } \boldsymbol{x} \in \partial\Omega_a. \end{aligned} \tag{4.9}$$

First, we consider the case $\nu_\pm = 1$, $\ell_+ = R_c$, and $l_- = r_c$, radius 1, where A has dimensionless radius r_c/R_c. This case can represent a partial block described in Figure 4.2(left). Under the scaling (4.8) the bounding circle B has dimensionless radius 1. We construct an asymptotic solution for small gap ε by first mapping the domain Ω in Figure 4.1(left) conformally into its image under the Möbius transformation of the two osculating circles A and B into concentric circles. To this end we move the origin of the complex plane to the center of the osculating circle B and set

$$w = w(z) = \frac{z - \alpha}{1 - \alpha z}, \tag{4.10}$$

where

$$\begin{aligned} \alpha = &-\frac{2\varepsilon R_c + 2R_c + \varepsilon^2 R_c + 2r_c\varepsilon + 2r_c}{2(\varepsilon R_c + r_c + R_c)} \\ &\pm \frac{\sqrt{\varepsilon(8R_c r_c + 4\varepsilon R_c^2 + 12\varepsilon R_c r_c + 4\varepsilon^2 R_c^2 + 8r_c^2 + 4\varepsilon^2 R_c r_c + \varepsilon^3 R_c^2 + 4\varepsilon r_c^2)}}{2(\varepsilon R_c + r_c + R_c)} \\ = &-1 \pm \sqrt{\frac{2r_c\varepsilon}{R_c + r_c}} + O(\varepsilon). \end{aligned} \tag{4.11}$$

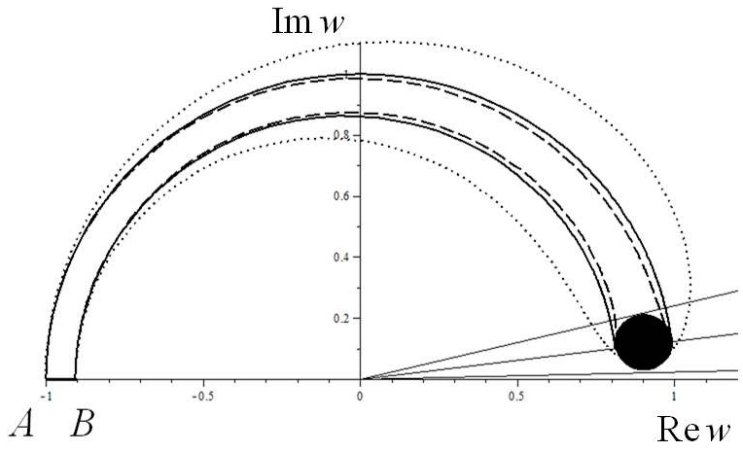

Fig. 4.3 *The image $\Omega_w = w(\Omega)$ of the (dimensionless) domain Ω in Figure* 4.1 *(left) under the conformal mapping* (4.10)*. The different necks in Figure* 4.1 *(right) are mapped onto the semi-annuli enclosed between the like-style arcs and the large disk in Ω is mapped onto the small black disk. The short black segment AB in Figure* 4.1 *(right) (of length ε) is mapped onto the thick black segment AB (of length $2\sqrt{\varepsilon} + O(\varepsilon)$). The rays from the origin are explained in the text below.*

The Möbius transformation (4.10) maps circle B into itself and Ω is mapped onto the domain $\Omega_w = w(\Omega)$ in Figure 4.3. The straits in Figure 4.1(left) are mapped onto the ring enclosed between the like-style arcs and the large disk is mapped onto the small black disk. The radius of the small black disk and the elevation of its center above the real axis are $O(\sqrt{\tilde{\varepsilon}})$. The short black segment of length ε in Figure 4.1(right) is mapped onto a segment of length $2\sqrt{\tilde{\varepsilon}} + O(\varepsilon)$.

Setting $u(z) = v(w)$ and $\tilde{\varepsilon} = 2r_c\varepsilon/(R_c + r_c)$, the system (4.9) is converted to

$$\Delta_w v(w) = -\frac{\ell_+^2}{D|w'(z)|^2} = -\frac{(4\tilde{\varepsilon} + O(\tilde{\varepsilon}^{3/2}))\ell_+^2}{D|w(1-\sqrt{\tilde{\varepsilon}}) - 1 + O(\tilde{\varepsilon})|^4} \text{ for } w \in \Omega_w, \tag{4.12}$$

$$\frac{\partial v(w)}{\partial n} = 0 \text{ for } w \in \partial\Omega_w - \partial\Omega_{w,a}, \quad v(w) = 0 \text{ for } w \in \partial\Omega_{w,a}.$$

The MFPT is bounded above and below by that from the inverse image of a circular ring cut by lines through the origin, tangent to the black disk at polar angles $\theta = c_1\sqrt{\tilde{\varepsilon}}$ (top) and $\theta = c_2\sqrt{\tilde{\varepsilon}}$ (bottom) for some positive constants c_1, c_2, independent of $\tilde{\varepsilon}$. Therefore, the MFPT from Ω equals that from the inverse image of a ring cut by an intermediate angle $\theta = c\sqrt{\tilde{\varepsilon}}$ (middle).

The asymptotic analysis of (4.12) begins with the observation that the solution of the boundary value problem (4.12) is to leading order independent of the radial variable in polar coordinates $w = re^{i\theta}$. Fixing $r = 1$, we impose the reflecting boundary condition at $\theta = c\sqrt{\tilde{\varepsilon}}$, where $c = O(1)$ is a constant independent of $\tilde{\varepsilon}$ to leading order, and the absorbing condition at $\theta = \pi$. The outer solution, obtained by a regular expansion of $v(e^{i\theta})$, is given by

$$v_0(e^{i\theta}) = A(\theta - \pi), \tag{4.13}$$

where A is an as yet undetermined constant. It follows that

$$\left.\frac{\partial v_0(e^{i\theta})}{\partial\theta}\right|_{\theta=\pi} = -A. \tag{4.14}$$

To determine A, we integrate (4.12) over the domain to obtain at the leading order

$$2\sqrt{\tilde{\varepsilon}}\left.\frac{\partial v_0(e^{i\theta})}{\partial\theta}\right|_{\theta=\pi} = -2\sqrt{\tilde{\varepsilon}}A \sim -\frac{|\Omega'|}{D}, \tag{4.15}$$

hence

$$A \sim \frac{|\Omega'|}{2D\sqrt{\tilde{\varepsilon}}}. \tag{4.16}$$

Now (4.13) gives for $\theta = c\sqrt{\tilde{\varepsilon}}$ the leading-order approximation (4.4). Returning to dimensional units, (4.4) becomes (4.5) and in the symmetric case $R_c = r_c$ (4.5) reduces to (4.6). ∎

Corollary. In the symmetric case with $\nu_+ = \nu_- > 1$ the curvature vanishes, that is, $R_c = r_c = \infty$. After scaling the boundary value problem (2.4)–(2.6) with (4.8), we can choose the bounding circles at A and B to have radius 1 and repeat the above analysis in the domain Ω_w enclosed by the dashed curves, shown in Figure 4.3. The result (4.6) becomes

$$\bar{\tau} = \frac{\pi|\,\Omega'|}{2D\sqrt{\varepsilon'/\ell_+}}[1 + o(1)] \ \text{ for } \varepsilon' \ll |\partial\Omega'|, \ell_+. \tag{4.17}$$

A more direct resolution of the boundary layer, based on the observation that the boundary layer equation (4.12) is an ordinary differential equation, is given in Holcman, Hoze, and Schuss (2011); Holcman and Schuss (2011); and Schuss (2013).

4.2. Exit from Several Bottlenecks. In the case of exit through any one of N well-separated necks with dimensionless curvature parameters l_j and widths $\tilde{\varepsilon}_j$, we construct the outer solution (4.13) at any one of the N absorbing windows so that (4.14) holds at each window. The integration of (4.12) over Ω gives the following analogue of (4.15):

$$\sum_{j=1}^{N} 2\sqrt{\tilde{\varepsilon}_j}\left.\frac{\partial v_0(e^{i\theta})}{\partial\theta}\right|_{\theta=\pi} = -\sum_{j=1}^{N} 2\sqrt{\tilde{\varepsilon}_j}A \sim -\frac{|\Omega'|}{D}; \tag{4.18}$$

hence

$$A \sim \frac{|\Omega'|}{2D\sum_{j=1}^{N}\sqrt{\tilde{\varepsilon}_j}}. \tag{4.19}$$

Equation (4.17) is then generalized to

$$\bar{\tau} = \frac{\pi|\Omega'|}{2D\sum_{j=1}^{N}\sqrt{\varepsilon'_j/\ell_j}}[1 + o(1)] \ \text{ for } \varepsilon'_j/\ell_j \ll |\partial\Omega|. \tag{4.20}$$

Equations (4.6) and (4.17) are generalized in a similar manner.

To calculate the exit probability through any one of the N necks, we apply the transformation (4.10) separately for each bottleneck at the absorbing images $\partial\Omega_{w,a_1},\dots,\partial\Omega_{w,a_N}$ to obtain images Ω_{w_j} for $j=1,2,\dots,N$. Then the probability of exiting through $\partial\Omega_{w,a_i}$ is the solution of the mixed boundary value problem (see Schuss (2010b, p. 185))

$$\Delta_w v(w)=0 \text{ for } w\in\Omega_{w_i},\quad \frac{\partial v(w)}{\partial n}=0 \text{ for } w\in\partial\Omega_{w_i}-\bigcup_{i=1}^{N}\partial\Omega_{w,a_i},\tag{4.21}$$
$$v(w)=1 \text{ for } w\in\partial\Omega_{w,a_i},\quad v(w)=0 \text{ for } w\in\partial\Omega_{w,a_j},\ j\neq i.$$

The outer solution, which is the exit probability through window $\partial\Omega_{w,i}$, is an unknown constant p_i. We construct boundary layers at each absorbing boundary $\partial\Omega_{w,a_j}$ for $j\neq i$ by solving the boundary value problem in Ω_{w_j}, which is of the type shown in Figure 4.3 with a neck of width ε_j. In each case the boundary layer is a linear function

$$v_j(\theta)=\delta_{i,j}-A_j(\theta-\pi) \text{ for all } j,\tag{4.22}$$

such that

$$v_j(0)\sim\delta_{i,j}+A_j\pi=p_i \text{ for all } j.\tag{4.23}$$

To determine the value of the constant p_i, we note that

$$\left.\frac{\partial v\left(e^{i\theta}\right)}{\partial n}\right|_{\partial\Omega_{w,a}}=\left.\frac{\partial v_j(\theta)}{\partial\theta}\right|_{\theta=\pi}=-A_j,\tag{4.24}$$

so the integration of (4.21) over Ω_{w_i} gives to leading order

$$\sum_{j=1}^{N}A_j|\partial\Omega_{w,a_j}|=\sum_{j=1}^{N}2A_j\sqrt{\bar{\varepsilon}_j}=0.\tag{4.25}$$

The $N+1$ equations (4.23) and (4.25) for the unknowns $p_i,A_1,\dots,A_N$ give the exit probability from an interior point in the planar case as

$$p_i=\frac{\sqrt{\varepsilon'/\ell_i}}{\sum_{j=1}^{N}\sqrt{\varepsilon'_j/\ell_j}}.\tag{4.26}$$

4.3. Bottlenecks. To calculate the MFPT $\bar{\tau}_{\boldsymbol{x}\to\partial\Omega_a}$, we need the following lemma.

LEMMA 4.2. *The* MFPT *from a point* $\boldsymbol{x}\in\Omega_1$ *to* $\partial\Omega_a$ *satisfies the renewal equation*

$$\bar{\tau}_{\boldsymbol{x}\to\partial\Omega_a}=\bar{\tau}_{\boldsymbol{x}\to\partial\Omega_i}+\int_{\partial\Omega_i}G(\boldsymbol{x}\,|\,\boldsymbol{\xi})\bar{\tau}_{\boldsymbol{\xi}\to\partial\Omega_a}\,dS_{\boldsymbol{\xi}},\tag{4.27}$$

where $G(\boldsymbol{x}\,|\,\boldsymbol{\xi})$ *is Green's function for the mixed boundary value problem*

$$\Delta u(\boldsymbol{x})=0 \text{ for } \boldsymbol{x}\in\Omega_1,\tag{4.28}$$
$$\frac{\partial u(\boldsymbol{x})}{\partial n}=0 \text{ for } \boldsymbol{x}\in\partial\Omega_1-\partial\Omega_i,\quad u(\boldsymbol{x})=\varphi(\boldsymbol{x}) \text{ for } \boldsymbol{x}\in\partial\Omega_i.$$

Proof. The identity follows from the fact that both sides of (4.27) satisfy (4.28) for $\boldsymbol{x}\in\Omega_1$ and coincide on $\partial\Omega_i$ (see Schuss (2010b, 2013)). ∎

Composite Domains. A planar composite domain with a bottleneck Ω consists of a head Ω_1 connected through a small interface $\partial\Omega_i$ to a narrow strip (neck) Ω_2. The boundary of Ω is assumed reflecting to Brownian particles, except the far end of Ω_2, denoted $\partial\Omega_a$, which is absorbing. For example, in Figure 2.1(left) the interface $\partial\Omega_i$ is the black segment AB and the absorbing boundary $\partial\Omega_a$ is the segment CD at the bottom of the strip. In higher dimensions the head Ω_1 is connected to a narrow cylindrical neck Ω_2.

THEOREM 4.3 (the NET from a domain with a long neck). *The* MFPT *of Brownian motion from a composite domain Ω with reflecting boundary to an absorbing boundary at the end of a narrow cylindrical neck of length L is given by*

$$\bar{\tau}_{\boldsymbol{x}\to\partial\Omega_a} = \bar{\tau}_{\boldsymbol{x}\to\partial\Omega_i} + \frac{L^2}{2D} + \frac{|\Omega_1|L}{|\partial\Omega_a|D}. \tag{4.29}$$

Proof. Consider the domain Ω in Figure 2.1. Lemma 4.2 indicates how to sum the MFPTs. To calculate $\bar{\tau}_{\partial\Omega_i\to\partial\Omega_a}$ and the absorption flux at the interface the boundary value problem

$$\Delta v(\boldsymbol{x}) = -\frac{1}{D} \text{ for } \boldsymbol{x}\in\Omega, \tag{4.30}$$

$$v(\boldsymbol{x}) = 0 \quad \text{for } \boldsymbol{x}\in\partial\Omega_a, \tag{4.31}$$

$$\frac{\partial v(\boldsymbol{x})}{\partial n(\boldsymbol{x})} = 0 \text{ for } \boldsymbol{x}\in\partial\Omega_r \tag{4.32}$$

has to be solved in the narrow neck Ω_2. A straightforward regular expansion of the solution in the cylindrical neck in powers of the neck radius shows that the solution can be approximated by that of the one-dimensional boundary value problem

$$Du_{zz} = -1 \text{ for } 0 < z < L, \quad u(0) = 0, \quad u(L) = u_H,$$

where the value at the interface $u(L) = u_H$ is as yet unknown. The solution is given by

$$u(z) = -\frac{z^2}{2D} + Bz, \tag{4.33}$$

so that

$$u(L) = u_H = -\frac{L^2}{2D} + b.l., \tag{4.34}$$

where $b.l.$ is a boundary layer term. Equation (4.34) relates the unknown constants B and u_H. The constant B is found by multiplying (2.4) by the Neumann function $N(\boldsymbol{x},\boldsymbol{y})$, integrating over Ω_1, applying Green's formula, and using the boundary conditions (4.31) and (4.32). Specifically, we obtain for all $\boldsymbol{y}\in\partial\Omega_i$

$$v(\boldsymbol{y}) = -\frac{1}{D}\int_{\Omega_1} N(\boldsymbol{x},\boldsymbol{y})\,d\boldsymbol{x} - \int_{\partial\Omega_i} N(\boldsymbol{x},\boldsymbol{y})\frac{\partial v(\boldsymbol{x})}{\partial n}\,dS_{\boldsymbol{x}} + \frac{1}{|\Omega_1|}\int_{\Omega_1} v(\boldsymbol{x})\,d\boldsymbol{x}. \tag{4.35}$$

Approximating, as we may, $v(\boldsymbol{y}) \approx u(L)$ and using (4.34), we obtain

$$-\frac{L^2}{2D} + b.l. = -\frac{1}{D}\int_{\Omega_1} N(\boldsymbol{x},\boldsymbol{y})\,d\boldsymbol{x} - \int_{\partial\Omega_i} N(\boldsymbol{x},\boldsymbol{y})\frac{\partial v(\boldsymbol{x})}{\partial n}\,dS_{\boldsymbol{x}} + \frac{1}{|\Omega_1|}\int_{\Omega_1} v(\boldsymbol{x})\,d\boldsymbol{x}. \tag{4.36}$$

Because $v(\boldsymbol{x})$ is the solution of the boundary value problem (2.4)–(2.6) in the entire domain $\Omega = \Omega_1 \bigcup \Omega_2$, the meaning of (4.36) is the connecting rule

$$\bar{\tau}_{\boldsymbol{x}\to\partial\Omega_a} = \bar{\tau}_{\boldsymbol{x}\to\partial\Omega_i} + \bar{\tau}_{\partial\Omega_i\to\partial\Omega_a}, \tag{4.37}$$

where

$$\bar{\tau}_{\boldsymbol{x}\to\partial\Omega_a} = \frac{1}{|\Omega_1|}\int_{\Omega_1} v(\boldsymbol{x})\,d\boldsymbol{x}, \tag{4.38}$$

$$\bar{\tau}_{\partial\Omega_i\to\partial\Omega_a} = u(L), \tag{4.39}$$

$$\bar{\tau}_{\boldsymbol{x}\to\partial\Omega_i} = -\frac{1}{D}\int_{\Omega} N(\boldsymbol{x},\boldsymbol{y})\,d\boldsymbol{x} - \int_{\partial\Omega_i} N(\boldsymbol{x},\boldsymbol{y})\frac{\partial v(\boldsymbol{x})}{\partial n}\,dS_{\boldsymbol{x}}. \tag{4.40}$$

Equation (4.38) gives the MFPT, averaged over Ω_1. The averaging is a valid approximation, because the MFPT to $\partial\Omega_i$ is constant to begin with (except in a negligible boundary layer). Equation (4.39) is the MFPT from the interface to the absorbing end $\partial\Omega_a$ of the strip, and (4.40) follows from the identity (Singer et al. (2006); Schuss (2013))

$$0 = \frac{1}{D}\int_{\Omega} N(\boldsymbol{x},\boldsymbol{\xi})\,d\boldsymbol{x} + \int_{\partial\Omega_a} N(\boldsymbol{x},\boldsymbol{\xi})g(\boldsymbol{x})\,dS_{\boldsymbol{x}} + C_\varepsilon \tag{4.41}$$

for all $\boldsymbol{\xi} \in \partial\Omega_a$. Matching the solutions in Ω_1 and Ω_2 continuously across $\partial\Omega_i$, we obtain the total flux on $\partial\Omega_i$ as

$$J = D\int_{\partial\Omega_i} \frac{\partial v(\boldsymbol{x})}{\partial \nu}\,dS_{\boldsymbol{x}} = -\left(|\Omega_1| + |\Omega_2|\right). \tag{4.42}$$

Noting that $\partial v(\boldsymbol{x})/\partial n = -u'(0) = -B$, we get from (4.42) for the different interfaces that

$$B = -\begin{cases} \dfrac{|\Omega_1|}{aD} + \dfrac{L}{D} & \text{for a line segment,} \\[2ex] \dfrac{|\Omega_1|}{2\pi aD} + \dfrac{L}{D} & \text{for a circle,} \\[2ex] \dfrac{|\Omega_1|}{\pi a^2 D} + \dfrac{L}{D} & \text{for a circular disk.} \end{cases} \tag{4.43}$$

Finally, we put (4.37)–(4.43) together to obtain (4.29). ∎

4.4. Two-Dimensional Bottlenecks. The expression (4.29) for the NET from a domain with a bottleneck in the form of a one-dimensional neck, such as a dendritic spine, can be summarized as follows. Consider a domain Ω with head Ω_1 and a narrow cylindrical neck Ω_2 of length L and radius a, connected smoothly to the head. The

radius of curvature at the connection is R_c. In the two-dimensional case,

(4.44)
$$\bar{\tau}_{\boldsymbol{x}\to\partial\Omega_a} = \begin{cases} \dfrac{|\Omega_1|}{\pi D}\ln\dfrac{|\partial\Omega_1|}{a} + \dfrac{O(1)}{D} + \dfrac{L^2}{2D} + \dfrac{|\Omega_1|L}{aD} \\ \text{planar spine connected to the neck at a right angle,} \\ \\ \dfrac{\pi|\Omega_1|}{D}\sqrt{\dfrac{R_c}{a}}\,(1+o(1)) + \dfrac{L^2}{2D} + \dfrac{|\Omega_1|L}{2\pi aD} \\ \text{planar spine with a smooth connecting funnel,} \\ \\ \dfrac{|\Omega_1|}{2\pi D}\log\dfrac{\sin\frac{\theta}{2}}{\sin\frac{\delta}{2}} + \dfrac{L^2}{2D} + \dfrac{|\Omega_1|L}{2\pi aD} \\ \text{spherical spine surface connected to the neck at a right angle,} \\ \dfrac{|\Omega_1|}{2D}\dfrac{\left(\dfrac{\ell}{(1+\nu)a}\right)^{\nu/1+\nu}\nu^{1/1+\nu}}{\sin\dfrac{\nu\pi}{1+\nu}} + \dfrac{L^2}{2D} + \dfrac{|\Omega_1|L}{2\pi aD} \\ \text{spherical spine surface with a smooth connecting funnel (4.3),} \end{cases}$$

where R is the radius of the sphere, $a = R\sin\delta/2$, and θ is the initial elevation angle on the sphere. If $|\Omega_1| \gg aL$ and $L \gg a$, the last term in (4.44) is dominant, which is the manifestation of the many returns of Brownian motion from the neck to the head prior to absorption at $\partial\Omega_a$. Further cases are considered in Schuss (2013). Note that modulation of neck length changes the residence time significantly.

4.5. References to Section 4. Section 4 develops a boundary layer theory for the solution of the mixed Neumann–Dirichlet problem for the Poisson equation in geometries in which the methodologies of Ward and Keller (1993); Ward, Henshaw, and Keller (1993); Ward and Van De Velde (1992); Kolokolnikov, Titcombe, and Ward (2005); Cheviakov, Ward, and Straube (2010); Coombs, Straube, and Ward (2009); Grigoriev et al. (2002); Holcman and Schuss (2004); Singer et al. (2006); Singer, Schuss, and Holcman (2006a,b); Singer and Schuss (2006); Bénichou and Voituriez (2008); and Schuss, Singer, and Holcman (2007) fail. In the case of sufficiently smooth boundaries near the absorbing window considered in Ward and Keller (1993); Ward, Henshaw, and Keller (1993); Ward and Van De Velde (1992); Kolokolnikov, Titcombe, and Ward (2005); Cheviakov, Ward, and Straube (2010); Coombs, Straube, and Ward (2009); and Bénichou and Voituriez (2008), the leading-order boundary layer problem is that of the exactly solvable electrified disk problem (Jackson (1975)), which gives no indication that the second-order asymptotics ansatz should be logarithmic. The Neumann function approach of Holcman and Schuss (2004); Singer et al. (2006); Singer, Schuss, and Holcman (2006a,b); Singer and Schuss (2006); and Schuss, Singer, and Holcman (2007), which is based on the standard leading-order singularity of Neumann's function (Garabedian (1964)), also fails to indicate the ansatz for second-order boundary layer expansion. It is the insight that Popov's Theorem 6.1 gives about the asymptotics of Neumann's function that points at the correct ansatz for both the boundary layer method and the Neumann function method in the smooth case.

In the geometries considered in section 4 the small Dirichlet part is located at the end of narrow straits with an absorbing end, connected smoothly to the Neumann boundary of the domain. The boundary layer near the absorbing boundary is not

mapped in an obvious way to an exactly solvable problem as in the smooth case. Conformal mapping replaces the standard local stretching in resolving the boundary layer in narrow necks. Additional problems related to Brownian motion in composite domains that contain a cylindrical narrow neck connected smoothly or sharply to the head are considered in Holcman and Schuss (2011). These include the asymptotic evaluation of the NET and of the leading eigenvalue in dumbbell-shaped domains and domains with many heads interconnected by narrow necks, the escape probability through any one of several narrow necks, and more.

The effect of obstacles on the diffusion constant has been studied in the biological context for the last two decades (Edidin, Kuo, and Sheetz (1991); Sheetz (1993); Suzuki and Sheetz (2001); Kusumi et al. (2005); Kusumi, Sako, and Yamamoto (1993); Saxton (1995); Saxton and Jacobson (1997); Eisinger, Flores, and Petersen (1986)) and more recently it was demonstrated, using single-particle imaging (Borgdorff and Choquet (2002); Tardin et al. (2003); Triller and Choquet (2003); Choquet (2010)), that the effective diffusion constant can span a large spectrum of values, from 0.001 to .2 $\mu\text{m}^2/\text{sec}$ (Choquet (2010)).

The calculation of the NET in composite domains with long necks was attempted in Korkotian, Holcman, and Segal (2004); Schuss, Singer, and Holcman (2007); Grigoriev et al. (2002); and Berezhkovskii, Barzykin, and Zitserman (2009), and ultimately accomplished in Holcman and Schuss (2011). The NET problem in a planar domain with an absorbing window at the end of a funnel was considered in Holcman, Hoze, and Schuss (2011). The case of planar domains that consist of large compartments interconnected by funnel-shaped bottlenecks was also considered in that paper, and the result (4.6) is found there too. The coarse-graining of diffusion into a Markov chain is discussed in Hänggi, Talkner, and Borkovec (1990) (see also Holcman and Schuss (2005); Holcman, Hoze, and Schuss (2011)). Finally, section 4 is based on Holcman, Hoze, and Schuss (2011).

5. A Brownian Needle in Dire Straits. As an application of the methodology described above, we study the planar diffusion of a stiff thin rod (needle) of length l in an infinite horizontal strip of width $l_0 > l$. This problem arises in modeling the repair process of a broken strand of DNA (Minsky (2004)). We assume that the rod is a long thin right circular cylinder with radius $a \ll l_0$ (Figure 5.1(left)). The planar motion of the rod is described by two coordinates of the centroid and the rotational angle θ between the axes of the strip and the rod. The y-coordinate of the center of the rod is measured from the axis of the strip. The motion of the rod is confined to the dumbbell-shaped domain Ω shown in Figure 5.1(right). The rod turns around if the point (θ, y) crosses from the left domain L into the right domain R or in the reverse direction, as described in Schuss (2010a). If

$$\varepsilon = \frac{l_0 - l}{l_0} \ll 1, \tag{5.1}$$

the window AB becomes narrow and the MFPTs $\tau_{\boldsymbol{L\to AB}}$ and $\tau_{\boldsymbol{R\to AB}}$, from the left or right domains to the segment AB, which is the stochastic separatrix SS, become much longer than those from AB to L or R. They also become independent of the starting position outside a boundary layer near the segment AB. Thus the definition of the time to turn around is independent of the choice of the domains L and R as long as they are well separated from the segment AB. The neck near the segment is the boundary layer region near $\theta = \pi/2$. We neglect henceforward the short times relative to the long ones.

To turn across the vertical position the rod has to reach the segment AB from the left domain L for the first time and then reach the right domain R for the first time, having returned to L any number of times prior to reaching R. The mean time to turn, $\tau_{\boldsymbol{L\to R}}$, is given asymptotically by Schuss (2010a) as

$$\tau_{\boldsymbol{L\to R}} \sim 2\tau_{\boldsymbol{L\to AB}} \quad \text{for } \varepsilon \ll 1. \tag{5.2}$$

The time to turn around is invariant to translations along the strip (the x-axis); therefore, it suffices to describe the rod movement by its angle θ and the y-coordinate of its center. The position of the rod is defined for $\theta \mod \pi$. Therefore, the motion of the rod in the invariant strip can be mapped into that in the (θ, y) planar domain Ω (see Figure 5.1(right)):

$$\Omega = \left\{(\theta, y) \,:\, |y| < \frac{l_0 - l\sin\theta}{2}, \quad 0 < \theta < \pi\right\}. \tag{5.3}$$

Our purpose is to calculate the mean turnaround time $\tau_{\boldsymbol{L\to R}}$.

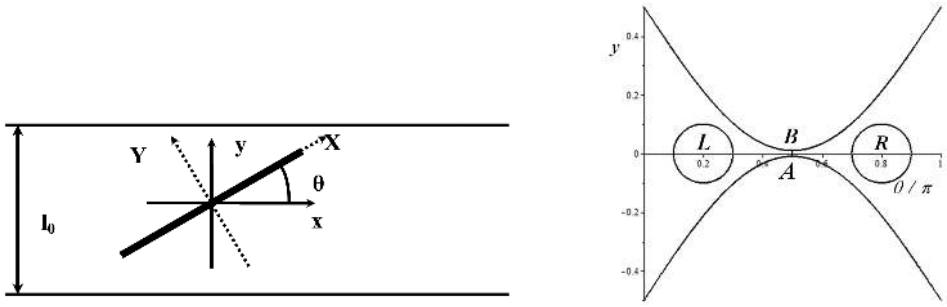

Fig. 5.1 *Rod in strip.* Left: *The strip width is l_0 and the rod length is $l < l_0$. The position of the rod is characterized by the angle θ and the fixed coordinates x and y and the rotating system of coordinates (X, Y, θ).* Right: *The motion of the rod is confined to the domain Ω in the (θ, y) plane.*

5.1. The Diffusion Law of a Brownian Needle in a Planar Strip. In a rotating system of coordinates (X, Y, θ), where the instantaneous X-axis is parallel to the long axis of the rod and the Y-axis is perpendicular to it, the diffusive motion of the rod is an anisotropic Brownian motion and can be described by the stochastic equations

$$\dot{X} = \sqrt{2D_X}\dot{w}_1, \quad \dot{Y} = \sqrt{2D_Y}\dot{w}_2, \quad \dot{\theta} = \sqrt{2D_r}\dot{w}_3,$$

where D_X is the longitudinal diffusion coefficient along the axis, D_Y the transversal diffusion constant, and D_r the rotational diffusion coefficient. Due to the anisotropy, the rod makes in general larger excursions in the X-direction than in the Y-direction, and this usually characterized by the ratio D_Y/D_X. Transforming into a fixed system of Cartesian coordinates (x, y), the translational and rotational motion of the centroid $(x(t), y(t))$ and the angle of rotation $\theta(t)$ of the rod are governed by the Itô equations

$$\begin{aligned} \dot{x} &= \cos(\theta)\sqrt{2D_X}\,\dot{w}_1 - \sin(\theta)\sqrt{2D_Y}\,\dot{w}_2, \\ \dot{y} &= \sin(\theta)\sqrt{2D_X}\,\dot{w}_1 + \cos(\theta)\sqrt{2D_Y}\,\dot{w}_2, \\ \dot{\theta} &= \sqrt{2D_r}\dot{w}_3, \end{aligned} \tag{5.4}$$

with conormal reflection at the boundary of the domain in Figure 5.1(bottom panel). Putting (5.4) in the matrix form

$$\dot{\boldsymbol{x}}(t) = \boldsymbol{B}(\theta)\,\dot{\boldsymbol{w}}, \tag{5.5}$$

where

$$\boldsymbol{x} = \begin{pmatrix} x \\ y \\ \theta \end{pmatrix}, \quad \boldsymbol{w} = \begin{pmatrix} w_1 \\ w_2 \\ w_3 \end{pmatrix},$$

and

$$\boldsymbol{B}(\theta) = \sqrt{2} \begin{pmatrix} \cos\theta & -\sin\theta & 0 \\ \sin\theta & \cos\theta & 0 \\ 0 & 0 & 1 \end{pmatrix} \begin{pmatrix} \sqrt{D_X} & 0 & 0 \\ 0 & \sqrt{D_Y} & 0 \\ 0 & 0 & \sqrt{D_r} \end{pmatrix},$$

we define the probability density function (pdf) $p(t, x, y, \theta)$ of the rod in the (x, y, θ) space by

$$p(t, x, y, \theta)\, d\boldsymbol{x} = \Pr\{(x(t), y(t), \theta(t)) \in \boldsymbol{x} + d\boldsymbol{x}\}, \tag{5.6}$$

which satisfies the Fokker–Planck equation (Schuss (2010b))

$$\frac{\partial p(t, \boldsymbol{x})}{\partial t} = -\nabla \cdot \boldsymbol{J}(t, \boldsymbol{x}),$$

where the flux is given by

$$\boldsymbol{J}(t, \boldsymbol{x}) = -\begin{pmatrix} \left[D_X \cos^2\theta + D_Y \sin^2\theta\right] \dfrac{\partial p}{\partial x} + \dfrac{1}{2}\left[(D_X - D_Y)\sin 2\theta\right] \dfrac{\partial p}{\partial y} \\ \left[D_X \sin^2\theta + D_Y \cos^2\theta\right] \dfrac{\partial p}{\partial y} + \dfrac{1}{2}\left[(D_X - D_Y)\sin 2\theta\right] \dfrac{\partial p}{\partial x} \\ D_r \dfrac{\partial p}{\partial \theta} \end{pmatrix}. \tag{5.7}$$

Because $\boldsymbol{J}(t, \boldsymbol{x})$ is π-periodic in θ and the position of the rod is defined modulo π, the boundary conditions are π-periodic in θ and the normal flux $-D_r \partial p(t, x, y, \theta)/\partial\theta$ is π-antiperiodic in θ.

The MFPT $\tau_{\boldsymbol{L}\to\boldsymbol{AB}}$ is the solution $u(\theta, y)$ of the PAV (Schuss (2010b)) boundary value problem

$$D_r \frac{\partial^2 u(\theta, y)}{\partial\theta^2} + D_y(\theta) \frac{\partial^2 u(\theta, y)}{\partial y^2} = -1 \ \text{ for } (\theta, y) \in \Omega_1, \tag{5.8}$$

where $D_y(\theta) = D_X \sin^2\theta + D_Y \cos^2\theta$ and $\Omega_1 = \Omega \cap \{\theta < \pi/2\}$, with the mixed boundary conditions

$$\frac{\partial u}{\partial \tilde{n}} = 0 \ \text{ for } (\theta, y) \ \text{ on the curved boundary and at } \theta = 0, \tag{5.9}$$

$$u\left(\frac{\pi}{2}, y\right) = 0 \ \text{ for } |y| < l_0 - l, \tag{5.10}$$

where the conormal derivative of $u(\theta, y)$ is given by

$$\frac{\partial u}{\partial \tilde{n}} = \nabla u(\theta, y) \cdot \tilde{\boldsymbol{n}}(\theta) \text{ for } (\theta, y) \text{ on the curved boundary} \tag{5.11}$$

and the conormal vector $\tilde{\boldsymbol{n}}(\theta)$ is given by

$$\tilde{\boldsymbol{n}}(\theta) = \begin{pmatrix} D_r & 0 \\ 0 & D_y(\theta) \end{pmatrix} \boldsymbol{n}(\theta), \tag{5.12}$$

with $\boldsymbol{n}(\theta)$ the unit outer normal vector at the curved boundary.

The MFPT is the solution of the PAV boundary value problem for (5.8)–(5.10), which corresponds to the stochastic system (5.5). Because the equation is translation-invariant with respect to x, it reduces to (5.8). The boundary conditions at a curved boundary for anisotropic diffusion with state-dependent diffusion tensor follow from Singer et al. (2008) and Schuss (2013, section 2.6.2).

5.2. The Turnaround Time. Equation (5.2) shows that it suffices to calculate the MFPT $\tau_{\boldsymbol{L}\to\boldsymbol{AB}}$ in order to calculate the turnaround time $\tau_{\boldsymbol{L}\to\boldsymbol{R}}$.

THEOREM 5.1 (the turnaround time). *The mean turnaround time of a Brownian needle of length l in a narrow strip of width l_0, such that $\varepsilon = (l_0 - l)/l_0 \ll 1$, is given by*

$$\tau_{\boldsymbol{L}\to\boldsymbol{R}} = \frac{\pi(\pi-2)}{D_r\sqrt{l_0(l_0-l)}}\sqrt{\frac{D_X}{D_r}}\left(1 + O\left(\sqrt{\frac{l_0-l}{l_0}}\right)\right). \tag{5.13}$$

Proof. Introducing the dimensionless variables

$$X' = \frac{X}{l_0}, \quad Y' = \frac{Y}{l_0}, \quad \xi(t) = \frac{x(t)}{l_0}, \quad \eta(t) = \frac{y(t)}{l_0}$$

and the normalized diffusion coefficients

$$D'_X = \frac{D_X}{l_0^2}, \quad D'_Y = \frac{D_Y}{l_0^2}, \quad D_\eta(\theta) = \frac{D_y(\theta)}{l_0^2},$$

we find that the domain Ω in (5.3) is mapped into

$$\Omega' = \left\{(\theta, \eta) \,:\, |\eta| < \frac{1-(1-\varepsilon)\sin\theta}{2}, \quad 0 < \theta < \pi\right\}. \tag{5.14}$$

To convert (5.8) to canonical form, we introduce the variable

$$\varphi(\theta) = \int_0^\theta \sqrt{\frac{D_\eta(\theta')}{D_r}}\, d\theta', \tag{5.15}$$

which defines the inverse function $\theta = \theta(\varphi)$, and set $u(\theta, y) = U(\varphi, \eta)$ to obtain

$$U_{\varphi\varphi}(\varphi,\eta) + U_{\eta\eta}(\varphi,\eta) = U_\varphi(\varphi,\eta)\sqrt{D_r}\,\frac{dD_\eta^{-1/2}(\theta)}{d\theta} - \frac{1}{D_\eta(\theta)}. \tag{5.16}$$

The domain Ω', defined in (5.14), is mapped into the similar domain

$$\Omega'' = \left\{(\varphi, \eta) \,:\, |\eta| < \frac{1-(1-\varepsilon)\sin\theta(\varphi)}{2}, \quad 0 < \varphi < \varphi(\pi)\right\} \tag{5.17}$$

in the (φ,η) plane. Because the conormal direction at the boundary becomes normal, so does the conormal derivative. The curved boundary in the scaled Figure 5.1(right) is denoted $\partial\Omega''$. It follows that the no-flux boundary condition (5.9) and the absorbing condition (5.10) become

$$\begin{aligned}&\frac{\partial U(\varphi,\eta)}{\partial n}=0 \text{ for } (\theta(\varphi),\eta) \text{ on } \partial\Omega'',\\ &\frac{\partial U(0,\eta)}{\partial\varphi}=0 \text{ for } |\eta|<\frac{1}{2},\quad U\left(\varphi\left(\frac{\pi}{2}\right),\eta\right)=0 \text{ for } |\eta|<\frac{\varepsilon}{2},\end{aligned} \tag{5.18}$$

respectively. The gap at $\theta=\pi/2$ is preserved and the (dimensionless) radius of curvature of the boundary at the gap is

$$R'=\frac{2D_\eta\left(\frac{\pi}{2}\right)}{(1-\varepsilon)D_r}=\frac{2D_X}{(1-\varepsilon)l_0^2D_r}. \tag{5.19}$$

First, we simplify (5.16) by setting

$$g(\varphi)=\sqrt{D_r}\,\frac{dD_\eta^{-1/2}(\theta)}{d\theta},\quad U(\varphi,\eta)=f(\varphi)V(\varphi,\eta) \tag{5.20}$$

and choosing $f(\varphi)$ such that $f'(\varphi)=\frac{1}{2}f(\varphi)g(\varphi)$. Note that

$$\left.\frac{dD_\eta^{-1/2}(\theta)}{d\theta}\right|_{\theta=0,\pi/2,\pi}=0. \tag{5.21}$$

Equation (5.16) becomes

$$V_{\varphi\varphi}+V_{\eta\eta}=\frac{1}{f(\varphi)}\left\{\left[g(\varphi)f'(\varphi)-f''(\varphi)\right]V-\frac{1}{D_\eta(\theta(\varphi))}\right\}. \tag{5.22}$$

Next, we move the origin to the center of curvature of the lower boundary by setting

$$\zeta=-\left(\eta-R'-\frac{\varepsilon}{2}\right)+i\left[\varphi-\varphi\left(\frac{\pi}{2}\right)\right]$$

and use the conformal mapping (4.10),

$$\omega=\frac{\zeta-R'\alpha}{R'-\alpha\zeta}, \tag{5.23}$$

with $\omega=\rho e^{i\psi}$. We also have

$$w'(\zeta)=\frac{1}{R'}\,\frac{(1+\alpha w)^2}{1-\alpha^2}, \tag{5.24}$$

$$|w'(\zeta)|^2=\frac{1}{R'^2}\left|\frac{(1+w\alpha)^2}{1-\alpha^2}\right|^2=\frac{|1-w+\sqrt{\varepsilon}\,w|^4}{4\varepsilon R'^2}(1+O(\sqrt{\varepsilon})). \tag{5.25}$$

The image Ω_ω of the domain Ω is given in Figure 5.2 and is similar to Ω_w in Figure 4.3, except for a small distortion near $\psi=c\sqrt{\varepsilon}$, which we neglect, as we may. Setting

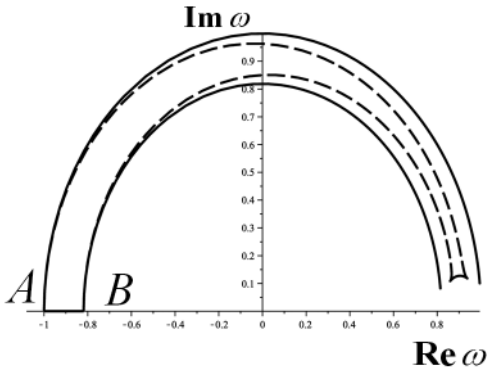

Fig. 5.2 *The image Ω_ω of the domain Ω under the mapping* (5.23)*. The values of the parameters are $\varepsilon = 0.01$ with the approximation $D_Y \ll D_X$. The domain is enclosed by the real segment AB, the dashed arcs, and the small closing cap. The solid circular arcs are the conformal images of arcs of the osculating circles at the narrow neck, as in Figure* 4.3*.*

$V(\varphi, \eta) = W(\rho, \psi)$, fixing $\rho = 1$ in Ω_ω, as in section 4, and abbreviating $W = W(\psi, 1)$, (5.22) becomes to leading order

$$W_{\psi\psi} + \frac{h(\psi)}{|\omega'(\zeta)|^2} W = -\frac{1}{|\omega'(\zeta)|^2 k(\psi)}, \tag{5.26}$$

where

$$h(\psi) = \left.\frac{f''(\varphi) - g(\varphi) f'(\varphi)}{f(\varphi)}\right|_{\rho=1}, \quad k(\psi) = f(\varphi) D_\eta(\theta(\varphi))|_{\rho=1}. \tag{5.27}$$

Using (4.12) and neglecting terms of order $O(\varepsilon)$, we rewrite (5.26) as

$$W_{\psi\psi} + \frac{4\varepsilon R'^2 h(\psi)}{|e^{i\psi}(1-\sqrt{\varepsilon}) - 1|^4} W = -\frac{4\varepsilon R'^2}{|e^{i\psi}(1-\sqrt{\varepsilon}) - 1|^4 k(\psi)}. \tag{5.28}$$

In view of (5.21), the boundary conditions (5.18) become

$$W_\psi(c\sqrt{\varepsilon}) = 0, \quad W(\pi) = 0. \tag{5.29}$$

The outer solution of (5.28) is a linear function $W_{\text{outer}}(\psi) = a\psi + b$, where a and b are as yet undetermined constants. The uniform approximation is constructed as $W_{\text{uniform}}(\psi) = W_{\text{outer}}(\psi) + W_{\text{bl}}(\psi)$, where the boundary layer $W_{\text{bl}}(\psi)$ is a function $Y(\xi)$ of the boundary layer variable $\xi = \psi/\sqrt{\varepsilon}$. The boundary layer equation is

$$Y''(\xi) + \frac{4R'^2 h(0)}{(1+\xi^2)^2} Y(\xi) = -\frac{4R'^2}{(1+\xi^2)^2 k(0)}, \tag{5.30}$$

which is simplified by the substitution $Y(\xi) = \tilde{Y}(\xi) + 1/h(0)k(0)$ to

$$\tilde{Y}''(\xi) + \frac{4R'^2 h(0)}{(1+\xi^2)^2} \tilde{Y}(\xi) = 0. \tag{5.31}$$

The boundary conditions (5.29) become $\tilde{Y}'(c) = 0$ and $\tilde{Y}(\infty) = 1/h(0)k(0)$.

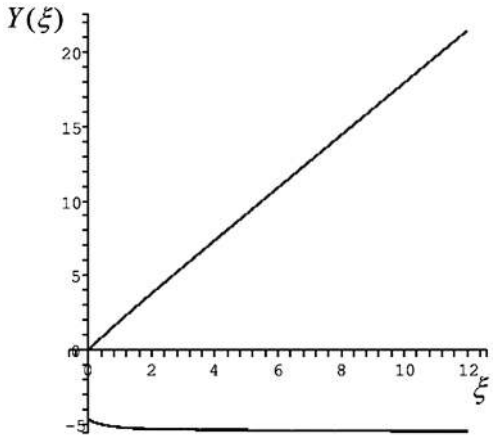

Fig. 5.3 *Two linearly independent solutions of* (5.31). *The linearly growing solution* $Y_1(\xi)$ *satisfies the initial conditions* $Y_1(0) = 0$, $Y_1'(0) = 2$. *The asymptotically constant solution* $Y_2(\xi)$ *satisfies the initial conditions* $Y_2(0) = -4.7$, $Y_2'(0) = -1$. *The asymptotic value is* $Y_2(\infty) \approx -5$.

The boundary layer equation (5.31) has two linearly independent solutions, $\tilde{Y}_1(\xi)$ and $\tilde{Y}_2(\xi)$, which are linear for sufficiently large ξ. Initial conditions for $\tilde{Y}_1(\xi)$ and $\tilde{Y}_2(\xi)$ can be chosen so that $\tilde{Y}_2(\xi) \to const$ as $\xi \to \infty$ (e.g., $\tilde{Y}_2(0) = -4.7$, $\tilde{Y}_2'(0) = -1$; see Figure 5.3). Thus the boundary layer function is given by

$$W_{\rm bl}(\psi) = A\tilde{Y}_1\left(\frac{\psi}{\sqrt{\varepsilon}}\right) + B\tilde{Y}_2\left(\frac{\psi}{\sqrt{\varepsilon}}\right) + C, \tag{5.32}$$

where A and B are constants to be determined and C is related to the constant $1/h(0)k(0)$ and is also determined below from the boundary and matching conditions.

The matching condition is that $W_{\rm bl}(\psi) = A\tilde{Y}_1(\psi/\sqrt{\varepsilon}) + B\tilde{Y}_2(\psi/\sqrt{\varepsilon}) + C$ remains bounded as $\xi \to \infty$, which implies $A = 0$. It follows that at the absorbing boundary $\psi = \pi$ we have

$$\begin{aligned} W_{\rm unif}(\pi) &= a\pi + b' = 0, \\ W_{\rm unif}'(\pi) &= a, \end{aligned} \tag{5.33}$$

where the constant b' incorporates all remaining constants. At the reflecting boundary we have to leading order

$$W_{\rm unif}'(c\sqrt{\varepsilon}) = W_{\rm outer}'(c\sqrt{\varepsilon}) + W_{\rm bl}'(c\sqrt{\varepsilon}) = a + B\frac{\tilde{Y}_2'(c)}{\sqrt{\varepsilon}} = 0, \tag{5.34}$$

which gives

$$B = -\frac{a\sqrt{\varepsilon}}{\tilde{Y}_2'(c)}, \quad b' = -a\pi. \tag{5.35}$$

The uniform approximation to $W(\omega)$ is given by

$$W_{\rm unif}(\rho e^{i\psi}) = a\left(\psi - \pi - \frac{\sqrt{\varepsilon}}{\tilde{Y}_2'(c)}\right), \tag{5.36}$$

so that using (5.20), (5.21), and (5.24) we obtain from (5.36)

$$\begin{aligned}\left.\frac{\partial u}{\partial n}\right|_{\zeta\in\partial\Omega_a} &= f\left(\varphi\left(\frac{\pi}{2}\right)\right)\left.\frac{\partial W(\rho e^{i\psi})}{\partial\psi}\right|_{\psi=\pi}\omega'(\zeta)\Big|_{\zeta=-1}\left.\frac{\partial\varphi}{\partial\theta}\right|_{\theta=\pi/2}\\ &= a\sqrt{\frac{2}{\varepsilon R'}}(1+O(\sqrt{\varepsilon})).\end{aligned} \tag{5.37}$$

Because $W(\omega)$ scales with $1/f(\varphi)$ relative to $V(\varphi,\eta)$, we may choose at the outset $f(\varphi(\pi/2))=1$.

Finally, to determine the value of a, we integrate (5.8) over Ω and use (5.37) and the fact that

$$\int_{\partial\Omega_a} dy = l_0\varepsilon$$

to obtain $a=-|\Omega|\sqrt{R'}/l_0D_r\sqrt{2\varepsilon}$. Now (5.36) gives the MFPT at any point $\boldsymbol{x}$ in the head as

$$\tau_{\boldsymbol{L}\to\boldsymbol{AB}} = u(\boldsymbol{x}) \sim W\left(\rho e^{ic\sqrt{\varepsilon}}\right) \sim -a\pi = \frac{\pi|\Omega|\sqrt{R'}}{l_0D_r\sqrt{2\varepsilon}}(1+O(\sqrt{\varepsilon}) \text{ for } \varepsilon\ll 1. \tag{5.38}$$

Reverting to the original dimensional variables, we get

$$\tau_{\boldsymbol{L}\to\boldsymbol{AB}} = \frac{\pi\left(\frac{\pi}{2}-1\right)}{D_r\sqrt{l_0(l_0-l)}}\sqrt{\frac{D_X}{D_r}}\left(1+O\left(\sqrt{\frac{l_0-l}{l_0}}\right)\right), \tag{5.39}$$

which, together with (5.2), is (5.13). □

6. NET in Bounded Domains in $\mathbb{R}^3$. The NET problem in three dimensions is more complicated than that in two dimensions, primarily because the singularity of Neumann's function for a regular domain is more complicated than (2.2).

6.1. The Neumann Function in Regular Domains in $\mathbb{R}^3$. The Neumann function $N(\boldsymbol{x},\boldsymbol{y})$ for a bounded domain $\Omega\subset\mathbb{R}^3$ with a sufficiently smooth boundary $\partial\Omega$ is the solution of the boundary value problem

$$\Delta_{\boldsymbol{x}}N(\boldsymbol{x},\boldsymbol{y}) = -\delta(\boldsymbol{x}-\boldsymbol{y}) + \frac{1}{|\Omega|} \text{ for } \boldsymbol{x},\boldsymbol{y}\in\Omega, \tag{6.1}$$

$$\frac{\partial N(\boldsymbol{x},\boldsymbol{y})}{\partial\nu_{\boldsymbol{x}}} = 0 \text{ for } \boldsymbol{x}\in\partial\Omega,\ \boldsymbol{y}\in\Omega, \tag{6.2}$$

where $\boldsymbol{\nu}(\boldsymbol{x})$ is the outer unit normal to the boundary $\partial\Omega$. If $\boldsymbol{x}$ or $\boldsymbol{y}$ (or both) are in $\partial\Omega$, then only half of any sufficiently small ball about a boundary point is contained in Ω, which means that the singularity of Neumann's function is $(2\pi|\boldsymbol{x}-\boldsymbol{y}|)^{-1}$. Therefore, Neumann's function for $\boldsymbol{y}\in\partial\Omega$ can be written as

$$N(\boldsymbol{x},\boldsymbol{y}) = \frac{1}{2\pi|\boldsymbol{x}-\boldsymbol{y}|} + v(\boldsymbol{x},\boldsymbol{y}), \tag{6.3}$$

where $v(\boldsymbol{x},\boldsymbol{y})$ satisfies

$$\Delta_{\boldsymbol{x}}v(\boldsymbol{x},\boldsymbol{y}) = \frac{1}{|\Omega|} \text{ for } \boldsymbol{x}\in\Omega,\ \boldsymbol{y}\in\partial\Omega. \tag{6.4}$$

In general, the Neumann function has the form (Garabedian (1964))

$$N(\boldsymbol{x},\boldsymbol{\xi}) = \frac{1}{4\pi|\boldsymbol{x}-\boldsymbol{\xi}|} + v_S(\boldsymbol{x},\boldsymbol{\xi}), \tag{6.5}$$

where $v_S(\boldsymbol{x},\boldsymbol{\xi})$ has a weaker singularity at $\boldsymbol{x}=\boldsymbol{\xi}$ when $\boldsymbol{x}\in\partial\Omega$ and $\boldsymbol{\xi}\in\Omega\cup\partial\Omega$ (see Theorem 6.1 below). It follows that only the singular part of the Neumann function contributes to the leading-order approximation to the solution of the integral equation (2.10). Thus we obtain for the leading-order approximation to the absorption flux density $g_0(\boldsymbol{x})$ on $\partial\Omega_a$ and for the leading-order approximation C_0 of the MFPT C the Helmholtz integral equation (2.10)

$$\frac{1}{2\pi}\int_{\partial\Omega_a}\frac{g_0(\boldsymbol{x})}{|\boldsymbol{x}-\boldsymbol{\xi}|}\,dS_{\boldsymbol{x}} = -C_0. \tag{6.6}$$

Here C_0 is a constant that represents the first approximation to the MFPT. It is also the electrostatic capacity of the window (Jackson (1975)).

The structure of Neumann's function for a regular domain in $\mathbb{R}^3$ is described in the following theorem (Popov (1992)).

THEOREM 6.1 (Popov). *Assume $\Omega\in\mathbb{R}^3$ is a bounded domain whose boundary $\partial\Omega$ has continuous partial derivatives up to order three. Then, for $\boldsymbol{z}\in\partial\Omega$, $\boldsymbol{y}\in\Omega\cup\partial\Omega$, the structure of the Neumann function (in dimensionless variables) is*

$$N(\boldsymbol{y},\boldsymbol{z}) = \frac{1}{2\pi|\boldsymbol{y}-\boldsymbol{z}|} - \frac{1}{8\pi}\left[L(\boldsymbol{z})+N(\boldsymbol{z})\right]\ln|\boldsymbol{y}-\boldsymbol{z}| + v_S(\boldsymbol{y},\boldsymbol{z}), \tag{6.7}$$

where $L(\boldsymbol{z})$ and $N(\boldsymbol{z})$ are the principal curvatures of $\partial\Omega$ at $\boldsymbol{z}$, and $v_S(\boldsymbol{y},\boldsymbol{z})$ is a bounded function of $\boldsymbol{x},\boldsymbol{y}$ in Ω.

Thus Neumann's function for a ball in $\mathbb{R}^3$ is found from the canonical representation of a hemisphere of (dimensionless) radius R at the south pole, $x_3 = R-\sqrt{R^2-(x_1^2+x_2^2)}$. We find that $L(\boldsymbol{z})=N(\boldsymbol{z})=\frac{1}{R}$, so for $|\boldsymbol{z}|=R$ we have

$$N(\boldsymbol{y},\boldsymbol{z}) = \frac{1}{2\pi|\boldsymbol{y}-\boldsymbol{z}|} + \frac{1}{4\pi R}\ln\frac{1}{|\boldsymbol{y}-\boldsymbol{z}|} + O(1). \tag{6.8}$$

Further analysis of the $O(1)$ term is given in Silbergleit, Mandel, and Nemenman (2003). The structure of Neumann's function for a ball is given in Kellog (1954, p. 247, Exercise 4).

6.2. Elliptic Absorbing Window. An explicit solution to the Helmholtz equation (6.6) can be found when the hole $\partial\Omega_a$ is an ellipse (Rayleigh (1945); Lurie (1964)). Consequently, the MFPT from a large cavity of volume $|\Omega|$ to a small elliptic absorbing window on an otherwise reflecting boundary $\partial\Omega$ can be calculated explicitly to leading order.

THEOREM 6.2. *Assume the boundary $\partial\Omega$ of a bounded domain $\Omega\subset\mathbb{R}^3$ is sufficiently regular and the absorbing boundary $\partial\Omega_a$ is the ellipse*

$$\frac{x^2}{a^2}+\frac{y^2}{b^2}\le 1, \quad z=0 \quad (b\le a). \tag{6.9}$$

If

$$\varepsilon = \left(\frac{|\partial\Omega_a|}{|\partial\Omega|}\right)^{1/2} \ll 1$$

and

$$\frac{|\Omega|^{2/3}}{|\partial\Omega|}, \frac{|\partial\Omega|}{|\Omega|^{2/3}} = O(1) \text{ for } \varepsilon \ll 1,$$

then the MFPT *from a* Ω *to* $\partial\Omega_a$ *is to leading order*

$$\mathbb{E}\tau(a,b) \sim \frac{|\Omega|}{2\pi Da} K(e), \tag{6.10}$$

where $K(\cdot)$ *is the complete elliptic integral of the first kind and* $e = \sqrt{1 - b^2/a^2}$ *is the eccentricity of the ellipse.*

If the hole is circular, $e = 0$ and $K(0) = \pi/2$, so that

$$\mathbb{E}\tau(a,a) \sim \frac{|\Omega|}{4Da} = O\left(\frac{1}{\varepsilon}\right). \tag{6.11}$$

If the hole is an elongated ellipse with $b \ll a$, the eccentricity is $e = \sqrt{1 - b^2/a^2} \simeq 1$, which gives the following asymptotic expansion for the elliptic integral (see Abramowitz and Stegun (1972, p. 591)):

$$K(e) \approx \frac{1}{2} \log\left(\frac{16}{1-e}\right). \tag{6.12}$$

Then (6.10) becomes

$$\mathbb{E}\tau(a,b) \sim \frac{|\Omega|}{2\pi Da} \log\left(\frac{4a}{b}\right), \tag{6.13}$$

showing that for $b \ll 1$ and $b \ll a$, the NET depends logarithmically on the short axis b.

A related problem is that of reaching a narrow spine-like absorbing or partially absorbing protrusion of the boundary into the domain. For the case of an ellipsoidal protrusion with transversal semiaxes $a_2 \geq a_1$ and height a_3, the eccentricity is $e = \sqrt{1 - a_1^2/a_2^2}$ with $f = a_3/a_1$. With the elliptic integral

$$K(e,f) = \frac{2}{\pi} \int_0^{\pi/2} \frac{d\theta}{\sqrt{(1 - e^2 \sin^2\theta)(1 + f^2 \tan^2\theta)}}, \tag{6.14}$$

the NET is given by Reingruber, Abad, and Holcman (2009) as

$$\bar{\tau} = \frac{|V|}{4a_1 D} K(e,f). \tag{6.15}$$

For $a_1 = a_2$ and $f = a_3/a_1$, the NET is

$$\bar{\tau} = \frac{|V|}{2\pi a_1 D} \begin{cases} \dfrac{\arccos f}{\sqrt{1 - f^2}}, & f \leq 1, \\ \dfrac{\operatorname{arccosh} f}{\sqrt{f^2 - 1}}, & f \geq 1. \end{cases} \tag{6.16}$$

In the limit $f \gg 1$, we obtain the approximation

$$\bar{\tau} \approx \frac{|V|}{2\pi a_1 D} \frac{\ln(2f)}{f}.$$

If the narrow protrusion is reflecting, except for N absorbing circular disks of radius s on its surface, the NET is given approximately by Reingruber, Abad, and Holcman (2009) as

$$\tau_{part-spine} = \frac{|V|}{4a_1 D} \frac{K(e,f)Ns + (1-\sigma)a_1}{Ns}. \tag{6.17}$$

The proof of Theorem 6.2 is based on the following lemma (see Lurie (1964)).

LEMMA 6.3 (Helmholtz (1860)). *Assume $\partial\Omega_a$ is the ellipse*

$$\frac{x^2}{a^2} + \frac{y^2}{b^2} \le 1, \quad z = 0 \quad (b \le a);$$

then the solution of the Helmholtz equation (6.6) *is*

$$g_0(\boldsymbol{x}) = \frac{\tilde{g}_0}{\sqrt{1 - \dfrac{x^2}{a^2} - \dfrac{y^2}{b^2}}}, \tag{6.18}$$

where $\tilde{g}_0$ is a constant.

The explicit solution of the Helmholtz equation for a general shaped window, such as a rectangle, is as yet unknown.

6.3. Second-Order Asymptotics for a Circular Window. To obtain higher-order asymptotics of the MFPT, we use Popov's Theorem 6.1 and Helmholtz's Lemma 6.3 in (2.10). We obtain the following theorem.

THEOREM 6.4. *Under the assumptions of Theorems* 6.1 *and* 6.2 *for a circular window of radius $a \ll |\partial\Omega|^{1/2}$,*

$$\mathbb{E}\tau = \frac{|\Omega|}{4aD\left[1 + \dfrac{L(\mathbf{0}) + N(\mathbf{0})}{2\pi} a\log a + o(a\log a)\right]} \quad \textit{for } a \ll |\partial\Omega|^{1/2}. \tag{6.19}$$

Proof. To obtain higher-order asymptotics of the MFPT, we us Popov's Theorem 6.1 and Helmholtz's Lemma 6.3 in (2.10), which, in view of (6.7), now becomes the generalized Helmholtz equation

$$\int_{\partial\Omega_a} g(\boldsymbol{x}) \left[\frac{1}{2\pi|\boldsymbol{x}-\boldsymbol{y}|} + H(\boldsymbol{x},\boldsymbol{y})\log|\boldsymbol{x}-\boldsymbol{y}| + O(1)\right] dS_{\boldsymbol{x}} = -C \ \text{ for } \boldsymbol{y} \in \partial\Omega_a,$$

$$H(\boldsymbol{x},\boldsymbol{y}) = -\frac{1}{8\pi}[L(\boldsymbol{y}) + N(\boldsymbol{y})] \sim -\frac{1}{8\pi}[L(\mathbf{0}) + N(\mathbf{0})] \ \text{ for } \boldsymbol{x},\boldsymbol{y} \in \partial\Omega_a, \ \varepsilon \ll 1, \tag{6.20}$$

where $L(\mathbf{0}), N(\mathbf{0})$ are the principal curvatures at the center $\mathbf{0}$ of $\partial\Omega_a$. To solve (6.20), we expand $g(\boldsymbol{x}) = g_0(\boldsymbol{x}) + g_1(\boldsymbol{x}) + g_2(\boldsymbol{x}) + \cdots$, where $g_{i+1}(\boldsymbol{x}) \ll g_i(\boldsymbol{x})$ for $\varepsilon \ll 1$, and choose

$$g_0(\boldsymbol{x}) = \frac{-2C}{a\pi\sqrt{1 - \dfrac{|\boldsymbol{x}|^2}{a^2}}}. \tag{6.21}$$

According to Lemma 6.3, if $\partial\Omega_a$ is a circular disk of radius a, then

$$\frac{1}{2\pi}\int_{\partial\Omega_a}\frac{g_0(\boldsymbol{x})}{|\boldsymbol{x}-\boldsymbol{y}|}\,dS_{\boldsymbol{x}} = C \quad \text{for all} \quad \boldsymbol{y}\in\partial\Omega_a. \tag{6.22}$$

It follows that $g_1(\boldsymbol{x})$ satisfies the integral equation

$$\frac{1}{2\pi}\int_{\partial\Omega_a}\frac{g_1(\boldsymbol{x})}{|\boldsymbol{x}-\boldsymbol{y}|}\,dS_{\boldsymbol{x}} = \frac{2C}{a\pi}\int_{\partial\Omega_a}\frac{H(\boldsymbol{x},\boldsymbol{y})\log|\boldsymbol{x}-\boldsymbol{y}|}{\sqrt{1-\dfrac{|\boldsymbol{x}|^2}{a^2}}}\,dS_{\boldsymbol{x}}. \tag{6.23}$$

Setting $y = a\boldsymbol{\eta}$, $\boldsymbol{x} = a\boldsymbol{\xi}$, and changing to polar coordinates in the integral on the right-hand side of (6.23), we obtain

$$\frac{1}{2\pi}\int_{\partial\Omega_a}\frac{g_1(\boldsymbol{x})}{|\boldsymbol{x}-\boldsymbol{y}|}\,dS_{\boldsymbol{x}} = \frac{2Ca^2}{a\pi}\int_0^{2\pi}d\theta\int_0^1\frac{H(a\boldsymbol{\xi},a\boldsymbol{\eta})\,[\log a+\log|\boldsymbol{\xi}-\boldsymbol{\eta}|]}{\sqrt{1-r^2}}\,r\,dr, \tag{6.24}$$

which gives in the limit $\varepsilon\to 0$ (e.g., keeping $|\Omega|$ fixed and $a\to 0$) that

$$\frac{1}{2\pi}\int_{\partial\Omega_a}\frac{g_1(\boldsymbol{x})}{|\boldsymbol{x}-\boldsymbol{y}|}\,dS_{\boldsymbol{x}} = -\frac{C[L(\boldsymbol{0})+N(\boldsymbol{0})]}{2\pi}\,a\log a + o(a\log a). \tag{6.25}$$

As in the pair (6.21), (6.22), we obtain that

$$g_1(\boldsymbol{x}) = \frac{-C[L(\boldsymbol{0})+N(\boldsymbol{0})]}{\pi^2\sqrt{1-\dfrac{|\boldsymbol{x}|^2}{a^2}}}\,\log a + o(\log a). \tag{6.26}$$

To determine the asymptotic value of the constant C, we recall that $g(\boldsymbol{x}) = \partial u(\boldsymbol{x})/\partial\nu$ and use in (2.7) the approximation

$$g(\boldsymbol{x}) \sim g_0(\boldsymbol{x}) + g_1(\boldsymbol{x}) \sim \frac{-2C}{a\pi\sqrt{1-\dfrac{|\boldsymbol{x}|^2}{a^2}}}\left[1+\frac{L(\boldsymbol{0})+N(\boldsymbol{0})}{2\pi}\,a\log a\right].$$

We obtain the NET (in dimensionless variables) as

$$\mathbb{E}\tau = \frac{|\Omega|}{4aD\left[1+\dfrac{L(\boldsymbol{0})+N(\boldsymbol{0})}{2\pi}\,a\log a + o(a\log a)\right]},$$

which is (6.19). □

Higher-order asymptotics of the principal eigenvalue of the Laplace equation in Ω with the mixed Dirichlet–Neumann boundary conditions (2.5)–(2.6) are derived from the asymptotic representation $\lambda_1(a)\sim(\mathbb{E}\tau)^{-1}$ for $a\ll|\partial\Omega|^{1/2}$, which gives

$$\lambda_1(a) = \frac{4aD}{|\Omega|}\left[1+\frac{L(\boldsymbol{0})+N(\boldsymbol{0})}{2\pi}\,a\log a + o(a\log a)\right]. \tag{6.27}$$

If Ω is a ball of radius R, then $L(\boldsymbol{0})+N(\boldsymbol{0}) = 2/R$ and the NET $\mathbb{E}\tau = C$ is given (in dimensional variables) by

$$\begin{aligned}\mathbb{E}\tau &= \frac{|\Omega|}{4aD\left[1-\dfrac{a}{\pi R}\log\dfrac{R}{a}+o\left(\dfrac{a}{R}\log\dfrac{R}{a}\right)\right]}\\ &= \frac{|\Omega|}{4aD}\left[1+\frac{a}{\pi R}\log\frac{R}{a}+o\left(\frac{a}{R}\log\frac{R}{a}\right)\right].\end{aligned} \tag{6.28}$$

Higher-order asymptotics for a ball can be obtained from Silbergleit, Mandel, and Nemenman (2003) and Kellog (1954, p. 247, Exercise 4). The principal eigenvalue for the Dirichlet problem in a domain with a small hole was considered in Ozawa (1981, 1983a,b).

7. The NET in a Solid Funnel-Shaped Domain. We consider now the NET problem in the solid of revolution obtained by rotating the symmetric domain Ω' in Figure 4.1(left) about its axis of symmetry. The absorbing end of the neck becomes a circular disk of radius $a' = \varepsilon'/2$.

THEOREM 7.1. *The* MFPT *to the absorbing boundary at the end of the funnel of a solid of revolution obtained by rotating the symmetric planar domain* (4.3) *of section* 4.1 *is given by*

$$\bar{\tau} = \frac{1}{\sqrt{2}}\left(\frac{\ell_+}{a'}\right)^{3/2}\frac{V}{\ell_+ D}(1+o(1)) \ \textit{for } a' \ll \ell_+, \tag{7.1}$$

where $V = |\Omega'|$ is the volume of the domain.

Proof. Due to cylindrical symmetry of the mixed boundary value problem (4.9), the MFPT in cylindrical coordinates centered on the axis of symmetry is independent of the angle. It follows that with the scaling (4.8) the boundary value problem (4.9) in the scaled spatial domain Ω can be written in cylindrical coordinates as

$$\Delta u = \frac{\partial^2 u}{\partial r^2} + \frac{1}{r}\frac{\partial u}{\partial r} + \frac{\partial^2 u}{\partial z^2} = -\frac{\ell_+^2}{D}. \tag{7.2}$$

Equation (7.2) can be considered as a two-dimensional problem in the planar cross-section by a plane through the axis of symmetry of Ω in the (r, z) plane. Here r is the distance to the axis of symmetry of Ω, the z-axis is perpendicular to that axis, and the origin is inside the cross-section of Ω, at the intersection of the axis with the tangent to the osculating circle to the cross-section at the gap. Setting $u_1 = ur^{1/2}$, the MFPT equation (7.2) takes the form

$$\frac{\partial^2 u_1(r,z)}{\partial r^2} + \frac{\partial^2 u_1(r,z)}{\partial z^2} = -\frac{\ell_+^2}{D}\left(r^{1/2} + \frac{u_1(r,z)}{4r^2}\right) \tag{7.3}$$

in the cross-section, with mixed Neumann–Dirichlet boundary conditions, as in the planar case. We assume that in dimensionless variables $\overline{AB} = \varepsilon \ll 1 < |\Omega|^{1/3}$, so the funnel is a narrow passage. The transformation to the rotated and translated coordinates is given by $\tilde{r} = r - 1 - \varepsilon/2,\ \tilde{z} = -z + 1$. Setting $u_1(r,z) = \tilde{u}(\tilde{r},\tilde{z})$, (7.3) becomes

$$\frac{\partial^2 \tilde{u}(\tilde{r},\tilde{z})}{\partial \tilde{r}^2} + \frac{\partial^2 \tilde{u}(\tilde{r},\tilde{z})}{\partial \tilde{z}^2} = -\frac{\ell_+^2}{D}\left(\left(\tilde{r}+1+\frac{\varepsilon}{2}\right)^{1/2} - \frac{\tilde{u}(\tilde{r},\tilde{z})}{4\left(\tilde{r}+1+\frac{\varepsilon}{2}\right)^2}\right). \tag{7.4}$$

The construction of the asymptotic expansion of the solution of the boundary layer equation (5.28) is similar to that in section 5.2. We construct an asymptotic solution for small gap ε by first mapping the cross-section in the (r, z) plane conformally into its image under the Möbius transformation (4.10),

$$w(\zeta) = \rho e^{i\eta} = \frac{\zeta - \alpha}{1 - \alpha\zeta}, \tag{7.5}$$

where α is given in (4.11) for the symmetric case $R_c = r_c = 1$. Setting $\tilde{u}(\zeta) = v(w)$, (7.4) becomes

(7.6)
$$\Delta_w v(w) = \frac{\ell_+^2}{D|w'(\zeta)|^2}\left(-\left|\mathcal{R}\mathrm{e}\frac{w+\alpha}{1+\alpha w}+1+\frac{\varepsilon}{2}\right|^{1/2} - \frac{v}{4\left|\mathcal{R}\mathrm{e}\dfrac{w+\alpha}{1+\alpha w}+1+\dfrac{\varepsilon}{2}\right|^2}\right).$$

Because the normalized head of Figure 4.1(left) is mapped into the narrow hot dog–shaped region in Figure 4.3 of width $\sqrt{\varepsilon}$ at $\rho = 1$, we approximate

$$w = e^{i\eta} + O(\sqrt{\varepsilon}), \quad \left|\frac{w+\alpha}{1+\alpha w}\right| = 1 + O(\sqrt{\varepsilon}). \tag{7.7}$$

We also have

$$w'(\zeta) = \frac{(1+\alpha w)^2}{\alpha^2-1}, \quad |w'(\zeta)|^2 = \frac{|1-w+\sqrt{\varepsilon}\,w|^4}{4\varepsilon}(1+O(\sqrt{\varepsilon})), \tag{7.8}$$

so that (7.3) reduces to

$$\Delta_w v = -\frac{\ell_+^2}{D}\frac{4\varepsilon(1+O(\sqrt{\varepsilon}))}{|1-w+\sqrt{\varepsilon}\,w|^4}\left(\sqrt{2}+\frac{1}{16}v\right) \tag{7.9}$$

or, equivalently,

$$v'' + \frac{\varepsilon}{4|e^{i\eta}-1-e^{i\eta}\sqrt{\varepsilon}|^4}v = \frac{\ell_+^2}{D}\frac{4\sqrt{2}\varepsilon}{|e^{i\eta}-1-e^{i\eta}\sqrt{\varepsilon}|^4}\left(1+O(\sqrt{\varepsilon})\right). \tag{7.10}$$

Setting $v = \ell_+^2(y - 16\sqrt{2})/D$, we obtain the leading-order equation

$$y''(\eta) + \frac{\varepsilon}{4|e^{i\eta}-1-e^{i\eta}\sqrt{\varepsilon}|^4}y(\eta) = 0. \tag{7.11}$$

The boundary conditions are

$$y'(c\sqrt{\varepsilon}) = 0, \quad y(\pi) = 16\sqrt{2}. \tag{7.12}$$

The outer solution is the linear function

$$y_{\text{outer}}(\eta) = M\eta + N, \tag{7.13}$$

where M and N are as yet undetermined constants. The absorbing boundary condition in (7.12) gives

$$y_{\text{outer}}(\pi) = M\pi + N = 16\sqrt{2}. \tag{7.14}$$

A boundary layer correction is needed to satisfy the boundary conditions at the reflecting boundary at $\eta = c\sqrt{\varepsilon}$. To resolve the boundary layer at $\eta = c\sqrt{\varepsilon}$, we set $\eta = \sqrt{\varepsilon}\xi$ and expand

$$\frac{\varepsilon^2}{|e^{i\eta}-1-e^{i\eta}\sqrt{\varepsilon}|^4} = \frac{1}{(1+\xi^2)^2} + O(\sqrt{\varepsilon}).$$

Writing $y_{\rm bl}(\eta) = Y(\xi)$, we obtain to leading order the boundary layer equation

$$Y''(\xi) + \frac{1}{4(1+\xi^2)^2} Y(\xi) = 0, \tag{7.15}$$

which has two linearly independent solutions, $Y_1(\xi)$ and $Y_2(\xi)$, that are linear functions for sufficiently large ξ. Initial conditions for $Y_1(\xi)$ and $Y_2(\xi)$ can be chosen so that $Y_2(\xi) \to const$ as $\xi \to \infty$ (e.g., $Y_2(0) = -4.7,\ Y_2'(0) = -1$; see Figure 5.3). Setting

$$y_{\rm bl}(\eta) = AY_1\left(\frac{\eta}{\sqrt{\varepsilon}}\right) + BY_2\left(\frac{\eta}{\sqrt{\varepsilon}}\right), \tag{7.16}$$

where A and B are constants to be determined, we seek a uniform approximation to $y(\eta)$ in the form $y_{\rm unif}(\eta) = y_{\rm outer}(\eta) + y_{\rm bl}(\eta)$. The matching condition is that $AY_1\left(\eta/\sqrt{\varepsilon}\right) + BY_2\left(\eta/\sqrt{\varepsilon}\right)$ remains bounded as $\xi \to \infty$, which implies $A = 0$. It follows that at the absorbing boundary $\eta = \pi$ we have

$$y_{\rm unif}(\pi) = M\pi + \beta - 5B = 16\sqrt{2}, \quad y'_{\rm unif}(\pi) = M. \tag{7.17}$$

At the reflecting boundary we have to leading order

$$y'_{\rm unif}(c\sqrt{\varepsilon}) = y'_{\rm outer}(c\sqrt{\varepsilon}) + y'_{\rm bl}(c\sqrt{\varepsilon}) = M + B\frac{Y_2'(c)}{\sqrt{\varepsilon}} = 0, \tag{7.18}$$

which gives

$$B = -\frac{M\sqrt{\varepsilon}}{Y_2'(c)}, \quad N = 16\sqrt{2} - \frac{5M\sqrt{\varepsilon}}{Y_2'(c)} - M\pi. \tag{7.19}$$

The uniform approximation to $v(w)$ is given by

$$v_{\rm unif}(\rho e^{i\eta}) = M\left(\eta - \pi - \frac{5\sqrt{\varepsilon}}{Y_2'(c)}\right), \tag{7.20}$$

so that, using (7.8), we obtain from (7.20)

$$\left.\frac{\partial u}{\partial n}\right|_{\zeta\in\partial\Omega_a} = \left.\frac{\partial v(\rho e^{i\eta})}{\partial \eta}\right|_{\eta=\pi} w'(\zeta)\Big|_{\zeta=-1} = \frac{2M}{\sqrt{\varepsilon}}(1 + O(\sqrt{\varepsilon})). \tag{7.21}$$

To determine the value of M, we integrate (4.9) over Ω and use (7.21) and the fact that

$$\int_{\partial\Omega_a} dS = \frac{\pi\varepsilon^2}{4} \tag{7.22}$$

to obtain $M = -2\ell_+^2|\Omega|/D\pi\varepsilon^{3/2}$. Then (7.20) gives the MFPT at any point $\boldsymbol{x}$ in the head as

$$\bar{\tau} = u(\boldsymbol{x}) \sim v\left(\rho e^{c\sqrt{\varepsilon}}\right) \sim 2\varepsilon^{-3/2}\frac{\ell_+^2|\Omega|}{D} = 2\varepsilon^{-3/2}\frac{|\Omega'|}{\ell_+ D} \ \text{ for } \varepsilon \ll 1. \tag{7.23}$$

The dimensional radius of the absorbing end of the funnel is $a' = \ell_+\varepsilon/2$ (see (4.8)), so (7.23) can be written in physical units as (7.1). ∎

The generalization of (7.1) to exit through N well-separated necks is found by noting that (7.22) becomes

$$\int_{\partial\Omega_a} dS = \sum_{j=1}^{N} \frac{\pi\varepsilon_j^2}{4}, \tag{7.24}$$

and the integration of (4.7) over Ω' gives the compatibility condition (dimensional)

$$\int_{\partial\Omega'} \frac{\partial u(\boldsymbol{x}')}{\partial n'}\, dS' = M \sum_{j=1}^{N} \frac{\ell_j \pi\varepsilon_j^2}{4\sqrt{\varepsilon_j}} = -\frac{|\Omega'|}{D}, \tag{7.25}$$

which determines

$$M = -\frac{4|\Omega'|}{D\sum_{j=1}^{N} \ell_j \pi\varepsilon_j^{3/2}}. \tag{7.26}$$

Hence, using the dimensional $a_j' = \ell_j\varepsilon_j/2$, we obtain

$$\bar{\tau} = -M\pi = \frac{1}{\sqrt{2}} \frac{|\Omega'|}{D\sum_{j=1}^{N} \ell_j \left(\dfrac{a_j'}{\ell_j}\right)^{3/2}}. \tag{7.27}$$

To calculate the exit probability from one of N necks, we note that the boundary layer function is to leading order linear, as in section 4.2. Therefore, in the three-dimensional case the exit probability is given by

$$p_i = \frac{\varepsilon_i^{3/2}\ell_i}{\sum_{j=1}^{N} \varepsilon_j^{3/2}\ell_j} = \frac{a_i'^{3/2}\ell_i^{-1/2}}{\sum_{j=1}^{N} a_j'^{3/2}\ell_j^{-1/2}}. \tag{7.28}$$

8. Selected Applications. A thorough review of the applications of the NET is given in Holcman and Schuss (2013). We illustrate below how the NET facilitates the analysis of certain chemical and biological models by coarse-graining the time scale and thus reducing the dimension of the parameter space. References for this section are given in section 8.3.

8.1. Transition Rate and the Principal Eigenvalue in Composite Domains. Consider, for simplicity, the sojourn time of Brownian motion in a compartment interconnected by a narrow neck with another compartment in a composite domain, as shown in Figure 1.1. The sojourn time is the MFPT from that compartment to another one. In the limit of shrinking neck, the sojourn time is to leading order independent of the initial point of the escaping trajectory and equals twice the MFPT from the compartment to the narrowest passage in the bottleneck (e.g., the interval $\boldsymbol{AB}$ in Figure 1.1). Indeed, the reciprocal of this MFPT is to leading order the rate at which trajectories reach the bottleneck from the first compartment, so the reciprocal of the MFPT is the lowest eigenvalue of the mixed Neumann–Dirichlet boundary value problem in the first compartment with Dirichlet conditions on the cross-section of the neck.

There is a spectral gap of order one from the smallest eigenvalue to the next one. Thus, it follows that long transition times of Brownian trajectories between compartments connected by bottlenecks are exponentially distributed and, therefore,

the leading eigenvalues of Neumann's problem for the Laplace equation in a domain that consists of compartments interconnected by narrow necks are to leading order the eigenvalues of a Markov chain with transition rates that are the reciprocals of the MFPTs through the narrow necks, as is the case for diffusion in a potential landscape with several deep wells (high barriers) (Schuss (2010b)). The evaluation of the leading eigenvalues of the Neumann problem for the Laplace equation in domains with bottlenecks reduces to the computation of the leading-order eigenvalues for the mixed Neumann–Dirichlet boundary value problem for the Laplace equation in domains with reflecting (Neumann) boundary, except for a small absorbing (Dirichlet) window at the end of a funnel.

8.1.1. The Principal Eigenvalue in a Domain with a Head and Narrow Neck. The composite domain Ω in Figure 2.1(left) consists of a head Ω_1 connected by a funnel to a narrow cylindrical neck Ω_2. The boundary of the domain is reflecting (Neumann) and only the far end of the cylinder $\partial\Omega_a$ is absorbing (Dirichlet). The left half of the dumbbell-shaped domain shown in Figure 1.1 is a composite domain of this type if the interval $\boldsymbol{AB}$ is an absorbing boundary. In the three-dimensional case the Dirichlet boundary $\partial\Omega_a$ is a small absorbing disk at the end of the cylinder. The domain Ω_1 is the one shown in Figure 4.1, and it is connected to the cylinder at an interface $\partial\Omega_i$, which in this case is the interval AB in Figure 4.1.

Using (4.29) and the fact that the principal eigenvalue of the mixed two- and three-dimensional Neumann-Dirichlet problems in domains with small Dirichlet and large Neumann parts of a smooth boundary is asymptotically the reciprocal of the MFPT, we find that the principal eigenvalue λ_1 in a domain with a single bottleneck is related to the MFPT through (Schuss (2010b, section 6.1))

$$\lambda_1 \sim \frac{1}{\bar{\tau}_{\boldsymbol{x}\to\partial\Omega_i} + \dfrac{L^2}{2D} + \dfrac{|\Omega_1|L}{|\partial\Omega_a|D}}, \tag{8.1}$$

where $\bar{\tau}_{\boldsymbol{x}\to\partial\Omega_i}$ is any one of the MFPTs given in (4.43), depending on the geometry of Ω_1. If a composite domain consists of a single head and N well-separated bottlenecks of different radii and neck lengths, then the reciprocal of the MFPT is the sum of the reciprocals of the NETs from a domain with a single bottleneck. That is, the principal eigenvalue λ_P is given by $\lambda_P \sim \sum_{j=1}^{N} \lambda_j$. This can be interpreted as the fact that the total efflux is the sum of N independent effluxes through the bottlenecks.

8.1.2. The Principal Eigenvalue and Coarse-Grained Diffusion in a Dumbbell. A dumbbell-shaped domain Ω consists of two- or three-dimensional compartments Ω_1 and Ω_3 and a connecting neck Ω_2 that is effectively one-dimensional, as shown in Figure 1.1. The stochastic separatrix (SS) in Ω is the locus of initial points for Brownian trajectories that are as equally likely to reach Ω_1 before Ω_3 as they are to reach Ω_3 before Ω_1. In Figure 1.1 the SS is the interval $\boldsymbol{AB}$. Consider the eigenvalue problem for the Laplace equation in Ω with Neumann boundary conditions.

THEOREM 8.1 (the principal eigenvalue in a dumbbell). *The smallest positive eigenvalue λ of the Neumann problem for the Laplace equation in the dumbbell is to leading order that of the two-state Markov process,*

$$\lambda = -(\lambda_{\mathrm{I}\to\mathrm{II}} + \lambda_{\mathrm{II}\to\mathrm{I}}),$$

where the transition rates from I *to* II *and from* II *to* I *are, respectively,*

$$\lambda_{\mathrm{I}\to\mathrm{II}} = \frac{1}{2\bar{\tau}_{\Omega_1\to SS}}, \quad \lambda_{\mathrm{II}\to\mathrm{I}} = \frac{1}{2\bar{\tau}_{\Omega_3\to SS}}. \tag{8.2}$$

Proof. We assume, as we may, that the SS is the cross-section of the neck at its center. Therefore the mean time to traverse the neck from Ω_1 to Ω_3 is asymptotically twice the MFPT $\bar{\tau}_{\boldsymbol{x}\to SS}$ from $\boldsymbol{x}\in\Omega_1$ to the SS (see Schuss (2010a)). This MFPT is to leading order independent of $\boldsymbol{x}\in\Omega_1$ and can be denoted $\bar{\tau}_{\Omega_1\to SS}$. Note that when the neck is narrow the mean residence time of a Brownian trajectory in Ω_1 or in Ω_3 is much longer than that in Ω_2. Also note that the FPT $\tau_{\boldsymbol{x}\to SS}$ for $\boldsymbol{x}\in\Omega_1$ is exponentially distributed for long times and so is $\tau_{\boldsymbol{x}\to SS}$ for $\boldsymbol{x}\in\Omega_3$ (Schuss (2010b)). Therefore, the Brownian motion in Ω can be coarse-grained into a two-state Markov process (a telegraph process), which is in State I when the Brownian trajectory is in Ω_1 and is in State II when it is in Ω_3. The state Ω_2 and the residence time there can be neglected relative to those in Ω_1 and Ω_3. The transition rates from I to II and from II to I, given in (8.2), can be found from (8.1), with L half the length of the neck and $SS=\partial\Omega_a$. The radii of curvature $R_{c,1}$ and $R_{c,3}$ at the two funnels may be different, and the domain is either Ω_1 or Ω_3.

The asymmetric Markovian random telegraph process jumps between two states, I and II, at independent exponentially distributed waiting times with rates $\lambda_{\mathrm{I}\to\mathrm{II}}$ and $\lambda_{\mathrm{II}\to\mathrm{I}}$, respectively. The transition pdf satisfies the linear differential equations[1] (Schuss (2010b))

$$\begin{aligned}\frac{\partial P\{I,t\,|\,x,t_0\}}{\partial t} &= -\lambda_{\mathrm{I}\to\mathrm{II}}P\{\mathrm{I},t\,|\,x,t_0\}+\lambda_{\mathrm{II}\to\mathrm{I}}P\{\mathrm{II},t\,|\,x,t_0\},\\ \frac{\partial P\{\mathrm{II},t\,|\,x,t_0\}}{\partial t} &= \lambda_{\mathrm{I}\to\mathrm{II}}P\{\mathrm{I},t\,|\,x,t_0\}-\lambda_{\mathrm{II}\to\mathrm{I}}P\{\mathrm{II},t\,|\,x,t_0\},\end{aligned}\tag{8.3}$$

which can be written in the obvious matrix notation as $\dot{\boldsymbol{p}}=\boldsymbol{A}\boldsymbol{p}$ with

$$\boldsymbol{A}=\begin{pmatrix}-\lambda_{\mathrm{I}\to\mathrm{II}} & \lambda_{\mathrm{II}\to\mathrm{I}}\\ \lambda_{\mathrm{I}\to\mathrm{II}} & -\lambda_{\mathrm{II}\to\mathrm{I}}\end{pmatrix}.$$

The eigenvalues of $\boldsymbol{A}$ are 0 with the normalized eigenvector $(\frac{1}{2},\frac{1}{2})^T$, and $-(\lambda_{\mathrm{I}\to\mathrm{II}}+\lambda_{\mathrm{II}\to\mathrm{I}})$ with the eigenvector $(1,-1)^T$. It follows that the nonzero eigenvalue of the system (8.3) is $\lambda=\lambda_{\mathrm{I}\to\mathrm{II}}+\lambda_{\mathrm{II}\to\mathrm{I}}$. Hence the theorem follows. ∎

For example, if the solid dumbbell consists of two general heads connected smoothly to the neck by funnels, the two rates are given by

$$\frac{1}{\lambda_{\mathrm{I}\rightleftarrows\mathrm{II}}}=\sqrt{2}\left[\left(\frac{R_{c,1/3}}{a}\right)^{3/2}\frac{|\Omega_{1/3}|}{R_{c,1/3}D}\right][1+o(1)]+\frac{L^2}{4D}+\frac{|\Omega_{1/3}|L}{\pi a^2 D}.\tag{8.4}$$

Next, we consider the Neumann problem for the Laplace equation in a domain that consists of any number of heads interconnected by narrow necks. The Brownian motion can be coarse-grained into a Markovian random walk that jumps between the connected domains at exponentially distributed times with rates determined by the FPTs and exit probabilities, as described in section 8.1.1. This random walk can in turn be approximated by an effective coarse-grained anisotropic diffusion, as done, for example, for atomic migration in crystals, for effective diffusion on a surface with obstacles (see the next section), and for a general diffusion on a potential landscape with deep wells.

[1] See http://en.wikipedia.org/wiki/Telegraph_process.

8.2. Coarse-Grained Diffusion on a Membrane Crowded with Obstacles. The second example is the organization of a cellular membrane, which is the determinant of molecular trafficking (e.g., receptors, lipids, etc.) to their destination. After decades of intense research on membrane organization it was demonstrated recently by single-particle imaging that the effective diffusion constant can span a large spectrum of values, from 0.001 to .2 μm^2/sec, yet it is still unclear how the heterogeneity of the membrane controls diffusion.

The degree of crowding of a membrane with obstacles can be estimated from diffusion data and from an appropriate model and its analysis, as explained below. The key to assessing the crowding is to estimate the local diffusion coefficient from the measured molecular trajectories and from the analytical formula for the MFPT through a narrow passage between obstacles. In a simplified model of crowding, the circular obstacles are as in Figure 8.1(a), which shows a square lattice of circular obstacles of radius a centered at the corners of lattice squares of side L. The MFPT

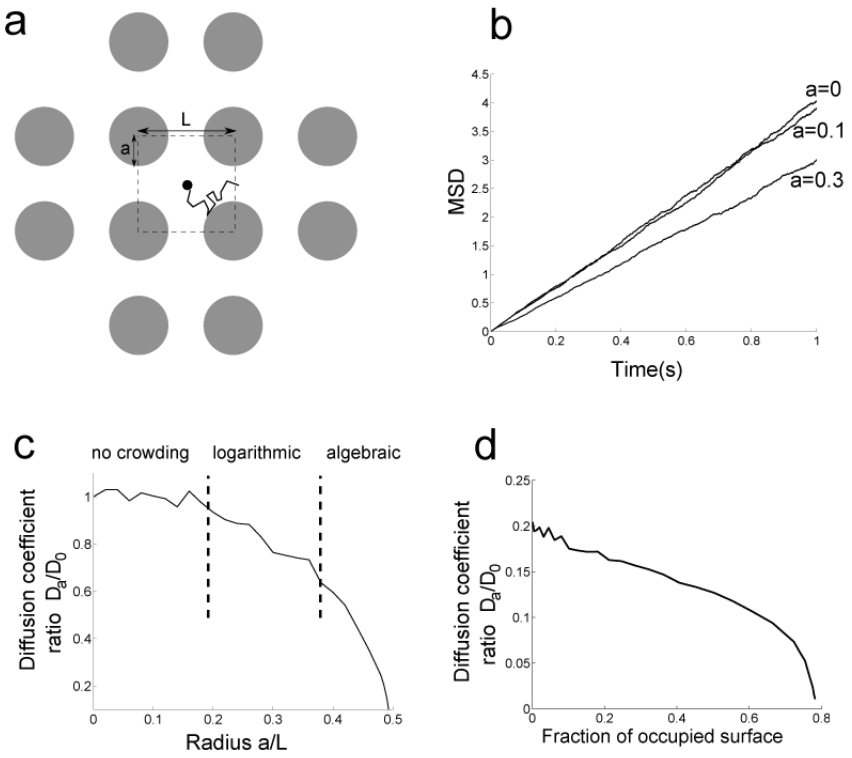

Fig. 8.1 A model of diffusion on a crowded membrane. (a) *Schematic representation of a Brownian particle diffusing in a crowded microdomain.* (b) *Mean square displacement* (MSD) *of the particle in a domain paved with microdomains. The* MSD *is linear, showing that crowding does not affect the nature of diffusion. The effective diffusion coefficient is computed from* $\langle \text{MSD}(t)/4t \rangle$. (c) *Effective diffusion coefficient computed from the* MSD *for different radii of the obstacles. Brownian simulations (continuous curve): there are three regions (separated by the dashed lines). While there is no crowding for* $a < 0.2$, *the decreasing of the effective diffusion coefficient for* $0.2 < a < 0.4$ *is logarithmic, and like square root for* $a > 0.4$. (d) *Effective diffusion coefficient of a particle diffusing in a domain as a function of the fraction of the occupied surface. An* AMPAR *has a diffusion coefficient of* $0.2\mu m^2$*/sec in a free membrane.*

$\bar{\tau}_4$ from a lattice box to the stochastic separatrix is (see Figure 8.1(a))

$$\bar{\tau}_4 = \frac{\bar{\tau}}{4}, \tag{8.5}$$

where $\bar{\tau}$ is the MFPT to a single absorbing window in the narrow straits with the other windows closed (reflecting instead of absorbing) (see Figure 2.1(left) or Figure 4.1(left)); thus $\bar{\tau}$ is the MFPT from the head to the segment $\boldsymbol{AB}$. It follows that the waiting time in the cell enclosed by the obstacles is approximately exponentially distributed with rate

$$\lambda = \frac{2}{\bar{\tau}_4}. \tag{8.6}$$

The asymptotic approximation to $\bar{\tau}$ is given by

$$\bar{\tau} \approx \begin{cases} c_1 & \text{for } 0.8 < \varepsilon < 1, \\ c_2|\Omega| \log \dfrac{1}{\varepsilon} + d_1 & \text{for } 0.55 < \varepsilon < 0.8, \\ c_3 \dfrac{|\Omega|}{\sqrt{\varepsilon}} + d_2 & \text{for } \varepsilon < 0.55, \end{cases} \tag{8.7}$$

with $\varepsilon = (L - 2a)/a$ and $d_1, d_2 = O(1)$ for $\varepsilon \ll 1$. The constants c_i $(i = 1, 2, 3)$ are calculated in Holcman, Hoze, and Schuss (2011). Thus the diffusion on the crowded membrane is coarse-grained into a symmetric Markovian jump process on a lattice with rate λ and step L. This, in turn, can be coarse-grained into a diffusion process in the plane with the effective diffusion coefficient $D = \lambda L^2/4 = 2L^2/\bar{\tau}$ (see Figure 8.1) (Schuss (1980); Hänggi, Talkner, and Borkovec (1990)).

8.3. References and Supplement to Section 8. The models and simulations of synaptic transmission are given in Freche et al. (2011); Taflia and Holcman (2011); and Holcman and Triller (2006). The microscopic model of reaction and diffusion follows Holcman and Schuss (2005) and Dao Duc and Holcman (2010). The results of section 8.1, concerning the principal eigenvalue in composite domains, are derived in Schuss (2013) and reviewed in Holcman and Schuss (2013). The stochastic separatrix is discussed in Ryter (1987a,b); and Schuss (2010a, 2013).

The principal eigenvalue for the Neumann problem in a dumbbell was derived in Schuss (2013) and reviewed in Holcman and Schuss (2013). The coarse-grained diffusion that describes atomic migration in crystals, mentioned at the end of this section, was derived in Schuss (1980, Chapter 8, section 2) and that for effective diffusion on a surface with obstacles, described in section 8.2, was derived in Holcman, Hoze, and Schuss (2011). A general coarse-graining of diffusion on a potential landscape with deep wells is given in Hänggi, Talkner, and Borkovec (1990). Some estimates of the asymptotic behavior of the leading eigenvalue in dumbbell-shaped domains are given in Arrieta (1995); Ward and Stafford (1999); Jimbo and Kosugi (2009); Dagdug et al. (2003); and references therein.

Membrane organization, as described in section 8.2, tries to explain what was recognized after decades of intense research (Edidin, Kuo, and Sheetz (1991); Sheetz (1993); Suzuki and Sheetz (2001); Kusumi et al. (2005); Kusumi, Sako, and Yamamoto (1993); Saxton (1995); Saxton and Jacobson (1997)) and demonstrated recently by single-particle imaging (Borgdorff and Choquet (2002); Tardin et al. (2003); Triller and Choquet (2003); Choquet (2010)), that the effective diffusion constant on the

membrane surface spans a wide range of values. The model shows how the heterogeneity of the membrane controls diffusion.

Applications to the calculation of the synaptic current, as described in Kandel, Schwartz, and Jessell (2000), are given in Taflia and Holcman (2011) and Freche et al. (2011). This current plays a fundamental role in neuronal communication: it is the direct and fast signal of synaptic transmission. It is argued that possible changes in the current dynamics are the result of synaptic plasticity, a process that underlies learning and memory (Kerchner and Nicoll (2008)).

Mathematical and physical models of the early steps of viral infection are constructed for the purposes of predicting and quantifying infectivity and the success of gene delivery (Holcman (2007); Lagache and Holcman (2008a,b); Amoruso, Lagache, and Holcman (2011); Lagache, Dauty, and Holcman (2009a)). The models give rise to rational Brownian dynamics simulations for the study of sensitivity to parameters and, eventually, for testing the increase or the drop in infectivity by using simultaneously a combination of various drugs. The modeling approach can be used for the optimization of the delivery in a high-dimensional parameter space (Lagache, Danos, and Holcman (2012)).

REFERENCES

M. Abramowitz and I. Stegun (1972), *Handbook of Mathematical Functions with Formulas, Graphs, and Mathematical Tables*, Dover, New York.

H. Adesnik, R.A. Nicoll, and P.M. England (2005), *Photoinactivation of native AMPA receptors reveals their real-time trafficking*, Neuron, 48, pp. 977–985.

C. Amoruso, T. Lagache, and D. Holcman (2011), *Modeling the early steps of cytoplasmic trafficking in viral infection and gene delivery*, SIAM J. Appl. Math., 71, pp. 2334–2358.

J.M. Arrieta (1995), *Rates of eigenvalues on a dumbbell domain. Simple eigenvalue case*, Trans. Amer. Math. Soc., 347, pp. 3503–3531.

M.C. Ashby, S.R. Maier, A. Nishimune, and J.M. Henley (2006), *Lateral diffusion drives constitutive exchange of AMPA receptors at dendritic spines and is regulated by spine morphology*, J. Neurosci., 26, pp. 7046–7055.

T. Aubin (1998), *Some Nonlinear Problems in Riemannian Geometry*, Springer-Verlag, New York.

O. Bénichou and R. Voituriez (2008), *Narrow-escape time problem: Time needed for a particle to exit a confining domain through a small window*, Phys. Rev. Lett., 100, 168105.

A.M. Berezhkovskii, A.V. Barzykin, and V.Yu. Zitserman (2009), *Escape from cavity through narrow tunnel*, J. Chem. Phys., 130, 245104.

A.J. Borgdorff and D. Choquet (2002), *Regulation of AMPA receptor lateral movements*, Nature, 417, pp. 649–653.

D.S. Bredt and R.A. Nicoll (2003), *AMPA receptor trafficking at excitatory synapses*, Neuron, 40, pp. 361–379.

P.C. Bressloff and J.M. Newby (2012), *Stochastic models of intracellular transport*, Rev. Modern Phys., 85, pp. 135–196.

S. Chandrasekhar (1943), *Stochastic problems in physics and astronomy*, Rev. Modern Phys., 15, pp. 2–89.

L. Chen, D.M. Chetkovich, R.S. Petralia, N.T. Sweeney, Y. Kawasaki, R.J. Wenthold, D.S. Bredt, and R.A. Nicoll (2000), *Stargazin regulates synaptic targeting of AMPA receptors by two distinct mechanisms*, Nature, 408, pp. 936–943.

A.F. Cheviakov, M.J. Ward, and R. Straube (2010), *An asymptotic analysis of the mean first passage time for narrow escape problems: Part* II: *The sphere*, Multiscale Model. Simul., 8, pp. 836–870.

D. Choquet (2010), *Fast AMPAR trafficking for a high-frequency synaptic transmission*, Eur. J. Neurosci., 32, pp. 250–260.

D. Coombs, R. Straube, and M. Ward (2009), *Diffusion on a sphere with localized traps: Mean first passage time, eigenvalue asymptotics, and Fekete points*, SIAM J. Appl. Math., 70, pp. 302–332.

L. Dagdug, A. M. Berezhkovskii, S.Y. Shvartsman, and G.H. Weiss (2003), *Equilibration in two chambers connected by a capillary*, J. Chem. Phys., 119, pp. 12473–12478.

K. Dao Duc and D. Holcman (2010), *Threshold activation for stochastic chemical reactions in microdomains*, Phys. Rev. E (3), 81 (4 Pt 1), 041107.
K. Dao Duc and D. Holcman (2012), *Using default constraints of the spindle assembly checkpoints to estimate the associated chemical rates*, BMC Biophys., 5:1.
B.A. Earnshaw and P.C. Bressloff (2006), *A biophysical model of AMPA receptor trafficking and its regulation during LTP/LTD*, J. Neurosci., 26, pp. 12362–12373.
M. Edidin, S.C. Kuo, and M.P. Sheetz (1991), *Lateral movements of membrane glycoproteins restricted by dynamic cytoplasmic barriers*, Science, 254, pp. 1379–1382.
J. Eisinger, J. Flores, and W.P. Petersen (1986), *A milling crowd model for local and long-range obstructed lateral diffusion. Mobility of excimeric probes in the membrane of intact erythrocytes*, Biophys J., 49, pp. 987–1001.
V.I. Fabrikant (1989), *Applications of Potential Theory in Mechanics*, Kluwer, Dordrecht, The Netherlands.
V.I. Fabrikant (1991), *Mixed Boundary Value Problems of Potential Theory and Their Applications in Engineering*, Kluwer, Dordrecht, The Netherlands, 1991.
D. Freche, U. Pannasch, N. Rouach, and D. Holcman (2011), *Synapse geometry and receptor dynamics modulate synaptic strength*, PLoS One, 6, e25122.
A. Gandolfi, A. Gerardi, and F. Marchetti (1985), *Diffusion-controlled reactions in two dimensions*, Acta Appl. Math., 4, pp. 139–159.
P.R. Garabedian (1964), *Partial Differential Equations*, Wiley, New York.
L.R. Gehlen, S. Nagai, K. Shimada, P. Meister, A. Taddei, and S.M. Gasser (2011), *Nuclear geometry and rapid mitosis ensure asymmetric episome segregation in yeast*, Biol., 21, pp. 25–33.
D. Gilbarg and N.S. Trudinger (2001), *Elliptic Partial Differential Equations of Second Order*, Springer-Verlag, New York.
U.F. Greber and M. Way (2006), *A superhighway to virus infection*, Cell, 124, pp. 741–754.
I.V. Grigoriev, Y.A. Makhnovskii, A.M. Berezhkovskii, and V.Y. Zitserman (2002), *Kinetics of escape through a small hole*, J. Chem. Phys., 116, pp. 9574–9577.
P. Hänggi, P. Talkner, and M. Borkovec (1990), *Reaction rate theory: Fifty years after Kramers*, Rev. Modern Phys., 62, pp. 251–341.
H.L.F. von Helmholtz (1860), *Theorie der Luftschwingungen in Röhren mit offenen Enden*, Crelle Bn., 57, pp. 1–72.
E. Hille (1976), *Analytic Function Theory*, Volume 1, Chelsea, New York.
D. Holcman (2007), *Modeling viral and DNA trafficking in the cytoplasm of a cell*, J. Statist. Phys., 127, pp. 471–494.
D. Holcman, K. Dao Duc, and K. Burrage (2013), *Successful Delivery of PTEN in the Cytoplasm Escaping from MicroRNAs Degradation*, preprint.
D. Holcman, N. Hoze, and Z. Schuss (2011), *Narrow escape through a funnel and effective diffusion on a crowded membrane*, Phys. Rev. E (3), 84, 021906.
D. Holcman and Z. Schuss (2004), *Escape through a small opening: Receptor trafficking in a synaptic membrane*, J. Statist. Phys., 117, pp. 191–230.
D. Holcman and Z. Schuss (2005), *Stochastic chemical reactions in microdomains*, J. Chem. Phys., 122, 114710.
D. Holcman and Z. Schuss (2008a), *Diffusion escape through a cluster of small absorbing windows*, J. Phys. A, 41, 155001.
D. Holcman and Z. Schuss (2008b), *Diffusion through a cluster of small windows and flux regulation in microdomains*, Phys. Lett. A, 372, pp. 3768–3772.
D. Holcman and Z. Schuss (2011), *Diffusion laws in dendritic spines*, J. Math. Neurosci., 1, 10.
D. Holcman and Z. Schuss (2012), *Brownian motion in dire straits*, Multiscale Model. Simul., 10, pp. 1204–1231.
D. Holcman and Z. Schuss (2013), *Control of flux by narrow passages and hidden targets in cellular biology*, Rep. Progr. Phys., 76, 074601.
D. Holcman and A. Triller (2006), *Modeling synaptic dynamics and receptor trafficking*, Biophys. J., 91, pp. 2405–2415.
J.D. Jackson (1975), *Classical Electrodynamics*, 2nd ed., Wiley, New York.
S. Jimbo and S. Kosugi (2009), *Spectra of domains with partial degeneration*, J. Math. Sci. Univ. Tokyo, 16, pp. 269–414.
F. John (1982), *Partial Differential Equations*, 4th ed., Appl. Math. Sci. 1, Springer, New York.
E.R. Kandel, J.H. Schwartz, and T.M. Jessell (2000), *Principles of Neural Science*, 4th ed., McGraw-Hill, New York.
O.D. Kellog (1954), *Foundations of Potential Theory*, Dover, New York.
G.A. Kerchner and R.A. Nicoll (2008), *Silent synapses and the emergence of a postsynaptic mechanism for LTP*, Nat. Rev. Neurosci., 9, pp. 813–825.

T. Kolokolnikov, M. Titcombe, and M.J. Ward (2005), *Optimizing the fundamental Neumann eigenvalue for the Laplacian in a domain with small traps*, European J. Appl. Math., 16, pp. 161–200.

E. Korkotian, D. Holcman, and M. Segal (2004), *Dynamic regulation of spine-dendrite coupling in cultured hippocampal neurons*, European J. Neurosci., 20, pp. 2649–2663.

A. Kusumi, C. Nakada, K. Ritchie, K. Murase, K. Suzuki, H. Murakoshi, R.S. Kasai, J. Kondo, and T. Fujiwara (2005), *Paradigm shift of the plasma membrane concept from the two-dimensional continuum fluid to the partitioned fluid: High-speed single-molecule tracking of membrane molecules*, Annu. Rev. Biophys. Biomol. Struct., 34, pp. 351–378.

A. Kusumi, Y. Sako, and M. Yamamoto (1993), *Confined lateral diffusion of membrane receptors as studied by single particle tracking (nanovid microscopy). Effects of calcium-induced differentiation in cultured epithelial cells*, Biophys J., 65, pp. 2021–2040.

T. Lagache, O. Danos, and D. Holcman (2012), *Modeling the step of endosomal escape during cell infection by a nonenveloped virus*, Biophys. J., 102, pp. 980–989.

T. Lagache, E. Dauty, and D. Holcman (2009a), *Physical principles and models describing intracellular virus particle dynamics*, Curr. Opin. Microbiol., 12, pp. 439–445.

T. Lagache, E. Dauty, and D. Holcman (2009b), *Quantitative analysis of virus and plasmid trafficking in cells*, Phys. Rev. E (3), 79, 011921.

T. Lagache and D. Holcman (2008a), *Effective motion of a virus trafficking inside a biological cell*, SIAM J. Appl. Math., 68, pp. 1146–1167.

T. Lagache and D. Holcman (2008b), *Quantifying intermittent transport in cell cytoplasm*, Phys. Rev. E (3), 77, 030901.

A.J. Lurie (1964), *Three-Dimensional Problems of the Theory of Elasticity*, Interscience Publishers, New York.

R. Malinow (2003), *AMPA receptor trafficking and long-term potentiation*, Philos. Trans. R. Soc. London Ser. B Biol. Sci., 358, pp. 707–714.

R. Malinow and R.C. Malenka (2002), *AMPA receptor trafficking and synaptic plasticity*, Annu. Rev. Neurosci., 25, pp. 103–126.

A. Minsky (2004), *Information content and complexity in the high-order organization of DNA*, Annu. Rev. Biophys. Biomol. Struct., 33, pp. 317–342.

B. Nadler, T. Naeh, and Z. Schuss (2001), *The stationary arrival process of independent diffusers from a continuum to an absorbing boundary is Poissonian*, SIAM J. Appl. Math., 62, pp. 433–447.

S. Ozawa (1981), *Singular variation of domains and eigenvalues of the Laplacian*, Duke Math. J., 48, pp. 767–778.

S. Ozawa (1983a), *An asymptotic formula for the eigenvalues of the Laplacian in a three dimensional domain with a small hole*, J. Fac. Sci. Univ. Tokyo Sect. IA Math., 30, pp. 243–257.

S. Ozawa (1983b), *Electrostatic capacity and eigenvalues of the Laplacian*, J. Fac. Sci. Univ. Tokyo Sect. IA Math., 30, pp. 53–62.

S. Pillay, M.J. Ward, A. Peirce, and T. Kolokolnikov (2010), *An asymptotic analysis of the mean first passage time for narrow escape problems: Part* I: *Two-dimensional domains*, Multiscale Model. Simul., 8, pp. 803–835.

L.S. Pontryagin, A.A. Andronov, and A.A. Vitt (1933), *On the statistical treatment of dynamical systems*, J. Theor. Exper. Phys., 3, pp. 165–180 (in Russian).

L.S. Pontryagin, A.A. Andronov, and A.A. Vitt (1989), *On the statistical treatment of dynamical systems*, Noise in Nonlinear Dynam., 1, pp. 329–340.

I.Yu. Popov (1992), *Extension theory and localization of resonances for domains of trap type*, Math. USSR Sb., 71, pp. 209–234.

J.W.S. Rayleigh (1945), *The Theory of Sound*, Vol. 2, 2nd ed., Dover, New York.

J. Reingruber, E. Abad, and D. Holcman (2009), *Narrow escape time to a structured target located at the boundary of a microdomain*, J. Chem. Phys., 130, 094909.

D. Ryter (1987a), *Noise-induced transitions in a double-well potential at low friction*, J. Statist. Phys., 49, pp. 751–765.

D. Ryter (1987b), *On the eigenfunctions of the Fokker-Planck operator and of its adjoint*, Phys. A, 142, pp. 103–121.

M.J. Saxton (1995), *Single-particle tracking: Effects of corrals*, Biophys. J., 69, pp. 389–398.

M.J. Saxton and K. Jacobson (1997), *Single-particle tracking: Applications to membrane dynamics*, Annu. Rev. Biophys. Biomol. Struct., 26, pp. 373–399.

Z. Schuss (1980), *Theory and Applications of Stochastic Differential Equations*, John Wiley & Sons, New York.

Z. Schuss (2010a), *Equilibrium and recrossings of the transition state: What can be learned from diffusion?*, J. Phys. Chem. C, 114, pp. 20320–20334.

Z. Schuss (2010b), *Theory and Applications of Stochastic Processes, and Analytical Approach*, Appl. Math. Sci. 170, Springer, New York.

Z. Schuss (2013), *Brownian Dynamics at Boundaries and Interfaces in Physics, Chemistry, and Biology*, Appl. Math. Sci., Springer, New York.

Z. Schuss, A. Singer, and D. Holcman (2007), *The narrow escape problem for diffusion in cellular microdomains*, Proc. Natl. Acad. Sci. USA, 104, pp. 16098–16103.

G. Seisenberger, M.U. Ried, T. Endress, H. Brüning, M. Hallek, and C. Bräuchle (2001), *Real-time single-molecule imaging of the infection pathway of an adeno-associated virus*, Science, 294, pp. 1929–1932.

M.P. Sheetz (1993), *Glycoprotein motility and dynamic domains in fluid plasma membranes*, Ann. Rev. Biophys. Biomol. Struct., 22, pp. 417–431.

S.H. Shi, Y. Hayashi, R.S. Petralia, S.H. Zaman, R.J. Wenthold, K. Svoboda, and R. Malinow (1999), *Rapid spine delivery and redistribution of AMPA receptors after synaptic NMDA receptor activation*, Science, 284, pp. 1811–1816.

A. Silbergleit, I. Mandel, and I. Nemenman (2003), *Potential and field singularity at a surface point charge*, J. Math. Phys., 44, pp. 4460–4466.

A. Singer and Z. Schuss (2006), *Activation through a narrow opening*, Phys. Rev. E (Rapid Comm.), 74, 020103(R).

A. Singer, Z. Schuss, D. Holcman, and R.S. Eisenberg (2006), *Narrow escape, Part* I, J. Statist. Phys., 122, pp. 437–463.

A. Singer, Z. Schuss, and D. Holcman (2006a), *Narrow escape, Part* II: *The circular disk*, J. Statist. Phys., 122, pp. 465–489.

A. Singer, Z. Schuss, and D. Holcman (2006b), *Narrow escape, Part* III: *Non-smooth domains and Riemann surfaces*, J. Statist. Phys., 122, pp. 491–509.

A. Singer, Z. Schuss, A. Osipov, and D. Holcman (2008), *Partially reflected diffusion*, SIAM J. Appl. Math., 68, pp. 844–868.

K. Suzuki and M.P. Sheetz (2001), *Binding of cross-linked glycosylphosphat-idylinositol-anchored proteins to discrete actin-associated sites and cholesterol-dependent domains*, Biophys. J., 81, pp. 2181–2189.

A. Taflia and D. Holcman (2011), *Estimating the synaptic current in a multiconductance AMPA receptor model*, Biophys. J., 101, pp. 781–792.

C. Tardin, L. Cognet, C. Bats, B. Lounis, and D. Choquet (2003), *Direct imaging of lateral movements of AMPA receptors inside synapses*, Embo J., 22, pp. 4656–4665.

A. Triller and D. Choquet (2003), *The role of receptor diffusion in the organization of the postsynaptic membrane*, Nat. Rev. Neurosci., 4, pp. 1251–1265.

M.J. Ward, W.D. Henshaw, and J.B. Keller (1993), *Summing logarithmic expansions for singularly perturbed eigenvalue problems*, SIAM J. Appl. Math., 53, pp. 799–828.

M.J. Ward and J.B. Keller (1993), *Strong localized perturbations of eigenvalue problems*, SIAM J. Appl. Math., 53, pp. 770–798.

M.J. Ward and D. Stafford (1999), *Metastable dynamics and spatially inhomogeneous equilibria in dumbbell-shaped domains*, Stud. Appl. Math., 103, pp. 51–73.

M.J. Ward and E. Van De Velde (1992), *The onset of thermal runaway in partially insulated or cooled reactors*, IMA J. Appl. Math., 48, pp. 53–85.